POLITECNICO DI TORINO

Facoltà di Ingegneria
Corso di Laurea Magistrale in Ingegneria dell'Autoveicolo

Tesi di Laurea Magistrale

Feasibility study of a wheel-legged unmanned ground vehicle

Academic Tutor:
Prof.ssa Massimiliana Carello

Company Tutors:
Ing. Massimo Milizia
Ing. Michele Settembrino

Candidate:
Davide Bergese

October 2022

Contents

1. Introduction

The thesis is focused on the feasibility study of a wheel-legged Unmanned Ground Vehicle UGV. It starts with an introduction about precision farming, specifically in the case analyzed the UGV task is to capture images from the ground through cameras and lidar sensors to recognize weeds and to value the crops when it is maturing in order to detect any problem in advance and avoid losses.

An overview of different suspensions adopted by rovers has been examined according to several parameters and the best fitting solution is chosen. After, comparing the original layout with different ones, the decision has been to select the original design changing the way how the actuation is performed.

Starting from the original design the implementation of the actuation was entirely redesigned opting for step motor to guide the rover's arm and the use of hub motors for the rover motion. After an iterative procedure in order to find the correct value of mass of the rover and the length of the arms, the torque needed for the rotative actuators has been computed and the CAD has been drawn.

A preliminary FEM analysis has been performed to evaluate the structural resistance with the design of the rover.

2. Rovers Overview

2.1. Context

In recent years, the growing use of technologies and automation has allowed the development of effective methods to carry out and withstand human activities. One of these businesses is surely precision farming, a management strategy based on information gathering technologies to acquire data and make agricultural production more efficient.

In the coming years, in fact, agriculture will have to meet a huge demand of food that could only be fulfilled using new technologies, such as robotic traps for insect pests and for sowing activities.

According to a Food and Agriculture Organization (FAO) estimate, in order to meet demand, in the year 2050 agriculture will have to produce almost 50% more food, feed and biofuels than in 2012. This estimate takes into account the recent projections of the United Nations (UN), which indicate how the world population could reach 9.73 billion in 2050. In sub-Saharan Africa and South Asia, agricultural production is expected to more than double by 2050 to meet rising demand, while in the rest of the world the expected increase would be about a third higher than current levels as shown in Table 1. Precision Farming is certainly today the most important tool available to meet these demands.

	2005/07	2050	2005/07 2012	2013-2050
World				
As projected in AT2050	100	159.6	14.8	44.8
With updated population projections (UN, 2015)	100	163.4	14.8	48.6
Sub-Saharan Africa and South Asia				
As projected in AT2050	100	224.9	20.0	104.9
With updated population projections (UN, 2015)	100	232.4	20.0	112.4
Rest of the world				
As projected in AT2050	100	144.9	13.8	31.2
With updated population projections (UN, 2015)	100	147.9	13.8	34.2

Table 1: Increase in agricultural production required to match projected demand

Precision Farming is a management system integrated with observations, measurements and actions, related to dynamic factors and variables in production systems. This process is necessary in order to analyze the data and consequently define a decision support system for the entire business management, with the aim of greater sustainability of climate and environmental, economic, productive and social improvements. In short, a system that provides the tools to perform the right actions, in the right place and at the right time [1].

Thanks to Precision Farming, it is possible to obtain economic and environmental benefits such as:

- optimization of inputs used as pesticides and fertilizers with consequent reduction in the use of water and air,
- reduction of water quantities for irrigation,
- rational use of decision-making factors, facilitating operators and reducing physical fatigue, work execution times, repetitive tasks and intensity, eliminating errors and maximizing profit (e.g., automatic guidance),
- controlled distribution according to the real needs of the crop (water, fertilizers, pesticides),
- use of sensors for real-time monitoring of crop health, control of the occurrence of phytopathogens or environmental conditions,
- reduction of the pressure exerted by agricultural systems on the environment,
- reduction of cultivation operations per unit of time and area, increase of unit yields,
- advanced traceability (Infotracing) from production to consumption and sale,
- historization and creation of online databases (cloud computing) for the development of Decision Support Systems (SSDs) for easier consultations,
- reduction of chemical infiltration in aquifers (leached N can be reduced by up to 75%),
- optimization of the required energy requirements,
- improved logistics of pre and post-harvest operations and rationalization of data per unit area.

An Italian startup has demonstrated what are the advantages obtainable with Precision Farming. The world produces 2 trillion dollars of food a year and 35% of this sum, 700 billion dollars, is lost before the harvest. To overcome this kind of problem, the Italian startup Agrorobotica - a project funded under the POR FESR Toscana 2014-2020, the regional development European found - has developed SpyFly, a robotic trap for monitoring insects, able to attract and capture the harmful ones during production and harvesting[1].

Thanks to proprietary recognition algorithms, SpyFly is able to:

- detect harmful insects,
- capture them through sexual calls to pheromones,
- send real-time alert messages to the farmer.

In addition, thanks to the Internet connection, crop monitoring can be viewed directly on the smartphone thanks to a specific application. The AI, on which SpyFly is based, is able to analyze the environmental data collected in the field and, thanks to the combination with data of harmful insects, the system develops and processes forward-looking models that can alert the farmer in advance of possible ideal conditions for the arrival of harmful insects.

Considering this high increase in demand, the total farming area under cultivation can only increase negligibly.

The European Parliament's Committee on Agriculture and Rural Development has also provided the same estimates (McIntyre 2015), highlighting the increase in world population and stressing the demand for healthy food and optimal nutritional values, which are the world's greatest future challenges.

In order to solve these issues, the agricultural sector tries to solve two potential problems:

- how to meet the increase in production with the lowest possible environmental impact,
- how to maintain high production levels with greater efficiency in the use of inputs.

The Strategic Plan for Innovation and Research in the Agricultural, Food and Forestry Sector provides four main guidelines for sustainability:

- the economic efficiency, profitability and sustainability of agricultural, livestock and forestry systems in different contexts,
- the conservation and reproduction of natural resources and biodiversity and the production of environmental services including climate change mitigation,
- the production of healthy and high-quality foods,
- relations between agriculture and local communities that ensure the quality of life in rural areas.

Europe, therefore, has the task of supporting and strengthening agricultural production by investing in its sustainability.

Developed technologies often do not meet the needs of farmers or cannot be used due to lack of Internet connection. For these reasons, much progress is still needed. Recent investment and new funding priorities, at Member State and EU level, offer encouraging signs.

Thanks to the Horizon 2020 Investment Framework Program, the European Commission is making around EUR 80 billion available over seven years for research and innovation.

On September 1st 2015, the Italian Minister of Agriculture, Food and Forestry Policies, Maurizio Martina, appointed a Working Group with the aim of increasing the sustainability of the Italian agricultural model through innovation in the short and long term. This will allow Italy to increase quality agricultural production and maintain the primacy of agrobiodiversity that distinguishes the country.

The objective is to reach by 2021 the 10% of the agricultural area cultivated in Italy through the use of technologies of precision agriculture, with the development of applications increasingly responsive to national agricultural production [2].

2.2. Requirements

The concept is to improve the efficiency of agriculture process and lowering the usage of pesticides by means of a collaborative interaction between an Unmanned Ground Vehicle (UGV) and a Fuel Cell Unmanned Aerial Vehicle (FCUAV). The idea is to implement a land rover that knows the ground conformation a priori thanks to a specific scan provided by the UAV, that collects the data with a Lidar Sensor. Thanks to this collaboration the rover can avoid the biggest obstacles due to the soil configuration and complete its task without any human intervention.

The main goal is to provide the kinematic and dynamic model equation of the chosen suspension and then, to dimension and design the components, including arms, actuators and dumping system. The suspension must be as stable as possible in order to avoid issue in case of different ground slopes, being capable of overcoming steps that may arise due to the roughness of the ground.

The UGV are systems that are originally designed to face extreme danger or inaccessible contexts. The rover must adapt to various kind of soil, obstacles and slopes. Generally, it is possible to divide the UGV into three main categories based on the propulsive means (as shown in the Figure 1):

- Tracks,
- Wheels,
- Legs,
- Hybrids.

Each of the afore mentioned has its own advantages and disadvantages in terms of energy consumption, speed and terrain adaptation.

Figure 1: From the upper left a tracked, wheeled and legged rover; at the bottom a hybrid one

2.3. Suspension types

In order to find the best possible solution, the first research is carried out to highlight a group of different types of suspensions with the aim of comparing them and finding advantages and disadvantages based on scenario upon shown.

The types of suspensions taken into account are:

- Rocker Bogie,
- Suspension with minimal actuation,
- Hylos' Suspension,
- Athlete's Suspension,
- Sherpa's Suspension,
- Sherpa TT's Suspension.

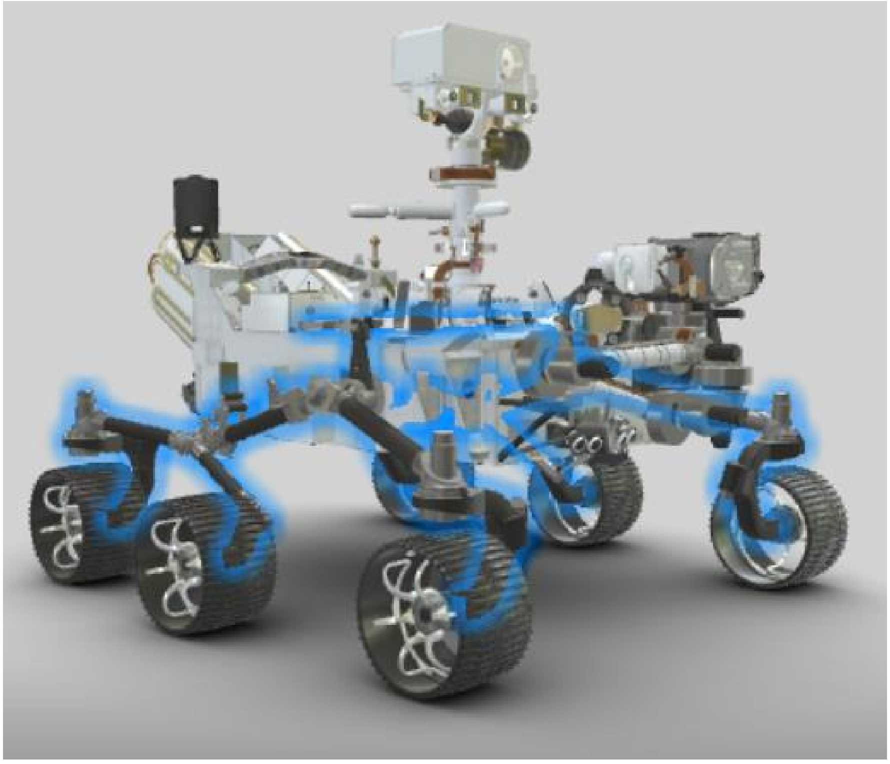

Figure 2: Nasa's Perseverance rocker bogie suspension system highlighted in blue

The Rocker Bogie mechanism is a consolidated choice of suspension for space applications, in fact many NASA's rovers exploring Mars have been equipped with it. Currently, it enables the space vehicle Perseverance to manage the rough Martian soil and it is shown in Figure 2.
The suspension system is the means of interaction between the wheels and the rover body. It consists of a single motor, a supporting frame with arms and joints, six wheels and a control circuitry [3]. Six wheels are needed in order to enlarge the contact surface with the terrain, and they are distributed symmetrical on both sides.
Three main components can be identified: the rocker, the bogie and the differential. The rocker consists of a rigid structure with two joints: one connects the differential with the wheels in the front and the other connects the former with the bogie in the back. There are two rockers: one on each side of the rover. In relation to the chassis, when one rocker rises, the other descends, therefore the two sides can move independently. It is called "rocker" because its objective is to balance the rover body, allowing it to "rock" up or down according to the positions of the wheels. The bogie connects the rear and middle wheels with the rocker. The expression "bogie" derives from old railroad systems, and it is used to refer to a carriage of multiple wheels which can rotate in order to allow the train to curve along the railways. Lastly, the differential joins the left and right rocker. This system has the capability to tilt without overturning. The tilt stability depends on the height of the center of gravity, as it happens in any suspension system. In the case of Martian rovers, they can incline up to 45° in

any direction however, this is limited to 30° for safety reasons [4,5]. The most important feature of this suspension system is that it does not include springs nor stub axles. As a consequence, the six wheels are able to remain on the ground even on irregular terrain, such as rocks or steps up to twice the wheel's diameter in size. The main weakness of this system is that it is designed for heavy vehicles, therefore it is optimized for slow speed. This limited pace is necessary in order to overcome obstacles and obtain enough torque to lift the heavy vehicle. In addition, if the vehicle is moving at higher speed and it stumbled across an impasse, the crash could seriously damage the structure. For these reasons, this system is designed for speed limited to 0.1 m/s [6].

The aforementioned configuration, known as passive rocker bogie mechanism, has the simplest design because it consists of only one motor and it utilizes a differential for rotation. The issue with this type is the difficulty in rotating. During the rotation the uneven load on wheels in the passive rocker bogie can throw the vehicle off balance. This is because the thrusting wheels have to sustain a heavier load than that on the pulling ones. In case of small turning radius, the wheels carrying the heavier weight can produce a force strong enough to lift the swingarms. The probability of occurrence of lifting the wheels and losing balance depends on the coefficient of friction between wheel and terrain, the turning radius, the linear speed of the vehicle and the rotational speed of the wheels.

However, this can be overcome adopting another configuration which supplies each wheel with a motor, consequently increasing the cost and the complexity of the mechanism [7]. On the other hand, it has the major benefit of always allowing an equal distribution of the weight on all wheels, despite the presence of obstacles. This enables the vehicle to turn more easily.

Another solution to the loss of balance due to the rotation is the active rocker bogie mechanism. This configuration equips each motor with DC motors controllers which independently allows speed regulation of the wheels. These controllers can slow down the wheels which otherwise would cause the lift of the vehicle. In fact, by reducing the speed of the pushing wheel, the rotating efficiency decreases as well. Predicting the instant when the wheel is about to lift is complex. This is done by measuring the angular position of the rocker through potentiometer and subsequently, calculating its derivative: the speed. An algorithm is used to compare the obtained speed with the maximum acceptable value. If the speed exceeds this value, the algorithm proceeds to reduce the speed of the pushing wheel. The active rocker bogie mechanism has the great advantage of avoiding vehicle lifting by controlling wheel speed. Nevertheless, the main drawback is to be able to distinguish when the wheel is about to lift or when it is simply overcoming an obstacle.

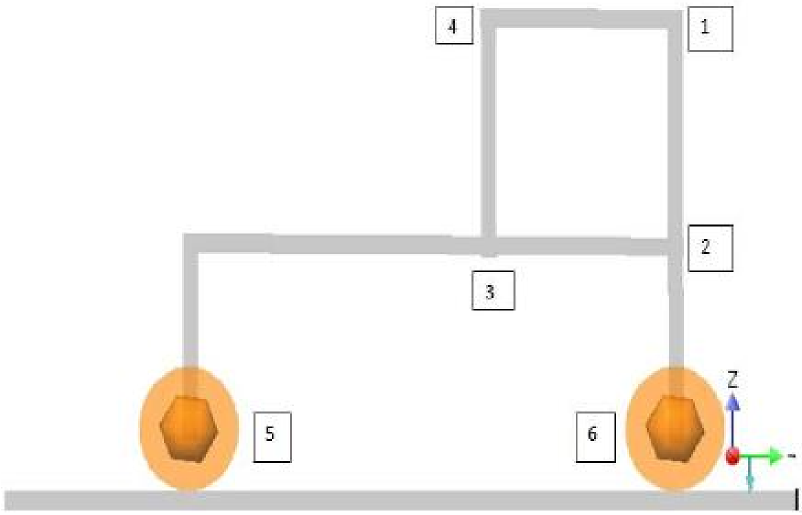

Figure 3: Four wheeled rover active suspension with minimal actuation

The suspension with minimal actuation (SMA) is implemented in a four-wheeled rover as shown in Figure 3. It derives from an attempt to remove one wheel from a five-wheeled passive suspension rover while reproducing the same motion by introducing active suspension. The advantages with respect to the already existing design are the reduction in weight and the better control of the kinematic movement. A system with more wheels has more freedom of mobility, however it has a higher mass which is not advisable for small rovers. The features of active suspension are open kinematic joints, which are simpler that the closed ones used in passive suspension, and the need for actuators and a control strategy to guarantee static stability. The five-wheeled passive suspension rover considered consists of a four bars mechanism called fork which is connected to the two front wheels. The two wheels in the back are connected to the chassis, as well as the back leg which is linked through a rotational joint managed by a spring with a high value of spring constant. This component is not present in all suspension system, and it enables the vehicle to better adapt to uneven soil while reversing. Using Grubler’s criterion, the degree of freedom for one of the two planes composing the system results to be two. One must be managed to keep the static stability and the other refers to the rotation of the wheel.

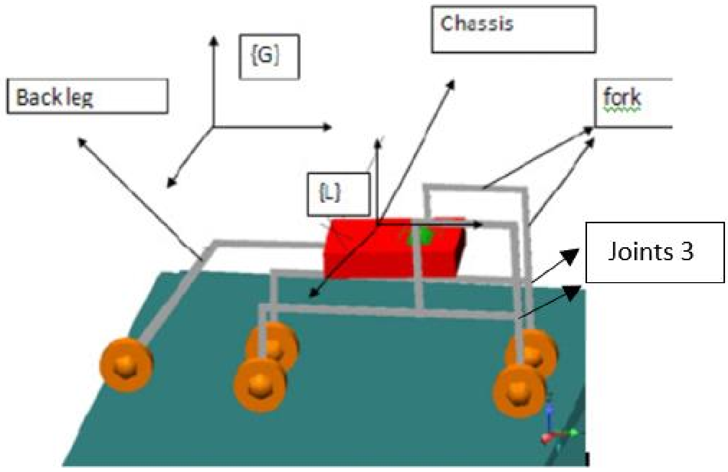

Figure 4: Five wheeled rover

The movement of the five wheeled rover showed in Figure 4 that has to be replicated on the four wheeled one is the following: when the front wheel encounters an obstacle the fork lifts then, because of the presence of a revolute joint number three, the structure of the fork changes in shape enabling a different distribution of the normal force which increases traction. As the second wheel mounts the obstacle, the fork returns to its previous configuration. During this movement the back wheel is used to stabilize the vehicle when it is climbing the obstacle and to prevent it from sliding backwards.

The four wheeled rover has to replicate the aforementioned movement, without the back leg and wheel. Despite the absence of one wheel, the number of degrees of freedom remains the same therefore, one joint must be actuated (only one if only one side is considered but, two actuators are needed in total). In this case the fourth joint is actuated in order to change the shape of the structure during the climb. Joints five and six are also active to drive the wheels, whereas the others are passive rotary ones. This active suspension system has two planar mechanisms connected by a differential rotary joint resembling the one in the rocker bogie suspension. Because of the actuation in joint four, when the first wheel starts climbing the configuration is changed and the joint turns anticlockwise, so that the front and back wheels move close to each other. When the second wheel gets over the obstacle the actuation system enables the joint four to turn clockwise and this allows the front and back wheel to outdistance each other. The control system is focused on the angular velocity of joint four. The dimension of the fork is what defines the capability of the vehicle to climb obstacles[8].

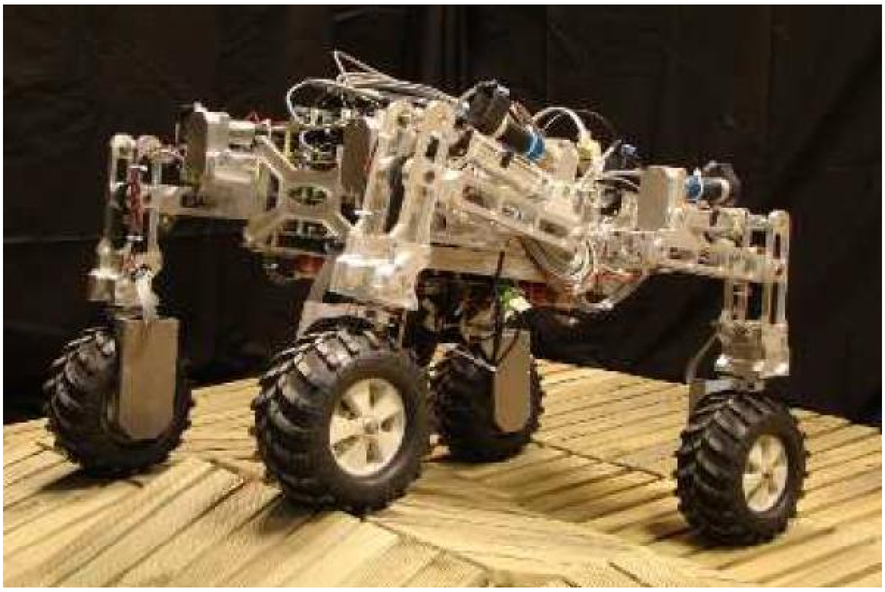

Figure 5: Hylos Rover

The Hylos[9] is high mobility redundantly hybrid UGV which adopts a hybrid wheel-legged active suspension as it can be seen in Figure 5. Its main objective is to ensure the contact patch between the wheel and the terrain in order to maintain the equilibrium of the rover. It has 16 degrees of freedom (dof), 4 for each leg since each of them has a 2 dof suspension, a steering mechanism and a driving wheel. This solution also allows to optimize the traction and to place the center of gravity (cog) of the UGV in optimal location based on the soil configuration in order to avoid reversals. One of the advantages that this solution offers is the possibility of overcoming obstacles having a height greater than its wheels diameter. This is achieved thanks to the actuators that move the suspension in such a fashion that allow the center of gravity of the system to be placed further from the obstacle, permitting the wheels in contact with the obstacle to step on it and after that the center of gravity is shifted towards the wheels that have already cleared the impediment so that also the other wheels are able to overtake it and the maneuver is completed.

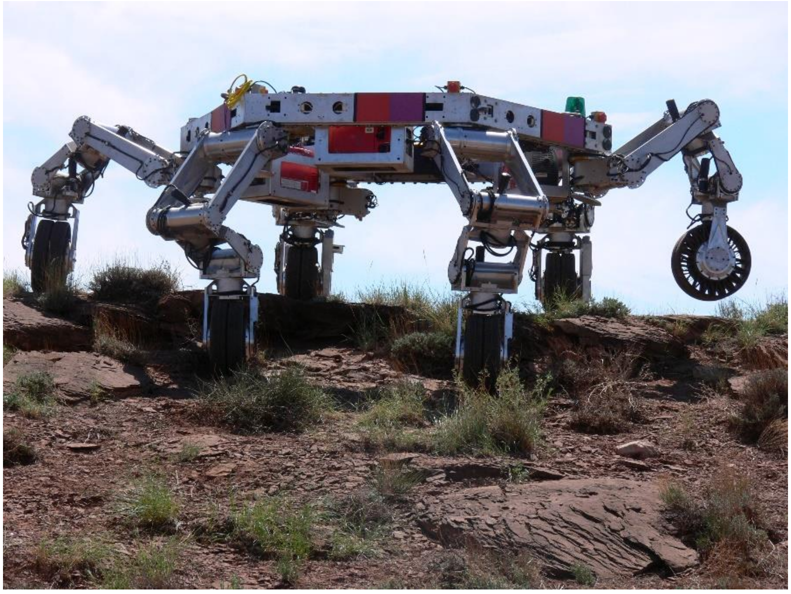

Figure 6: Athlete Rover

Athlete is the All-Terrain Hex-Limbed Extra-Terrestrial Explorer is showed in Figure 6 designed and built at JPL laboratories (NASA). Its original purpose is to assist human exploration of the Moon by transporting cargo on the hostile terrain of Earth's satellite. This vehicle is three meters in diameter and consists of six Degrees-of-Freedom limbs with a wheel at each end. They are referred to as limbs and not legs because each can be equipped with a tool. For instance, thanks to a tool adapter at the end of one limb, a gripper can be connected to and actuated by the wheel: the motor inside the wheel makes it turn, and this allows the opening or closure of the gripper. The increase in weight due to the tools is balanced by the reduction caused by the small size of the wheels, compared to that of other planetary exploration rovers such as Opportunity. Every wheel has a motor inside, and, because of the limited dimension of the wheels, the motors can be lighter and smaller as well. The limbs are linked to a hexagonal structure which has two cameras on every size. This enables the operator, controlling the motion remotely from the Earth or astronauts on the Moon, to have a complete view for better mobility [10]. The wheels can either be used to roll on the ground, or they can be locked rotationally in order to walk over obstacles and enable a walking gait. In fact, this vehicle is considered as a combination of a wheeled rover and a walking robot thanks to a system called Sliding Gait.

The possibility of two modes, driving and walking, increase the complexity, on the other hand, it allows the vehicle to adapt to different types of terrain, enabling it to be more flexible. When rolling is not possible, Sliding Gait allows some wheels to be relocated, to overcome an obstacle for instance, while the others are used as anchors. During these maneuvers all six wheels keep contact with the ground. The algorithm on which Sliding Gait is based allows to reposition the wheel and shift the payload at the same time, in order to keep it stable. However, the center of gravity is barely affected by this change in position, which is an advantage, because it lowers the risk of slipping [11]. The rolling capability of the rover is set up with a single command. Moreover, while rolling the rover can maintain its frame level and wheels coordinated by setting an active obedience to the commands. Nevertheless, in the presence of a step this active response is not available and consequently, the movement needs to be set by the operator, which can be a laborious task. To overcome this a decision support software, called FootFall, has been developed. It aims at creating the commands to enable the rover to step and walk on rough soil. FootFall uses the cameras on board the vehicle to create a 3D map of the terrain and shares it with the operator to increase their awareness of the surroundings. The latest version of the software is able to crate the command to overcome only one step at a time: when the operator decides where to position the leg, the software generates a trajectory checking the absence of collisions and respecting kinematic and safety restrictions. The sequence of commands obtained can ultimately be adjusted by the operator before been actuated [12].

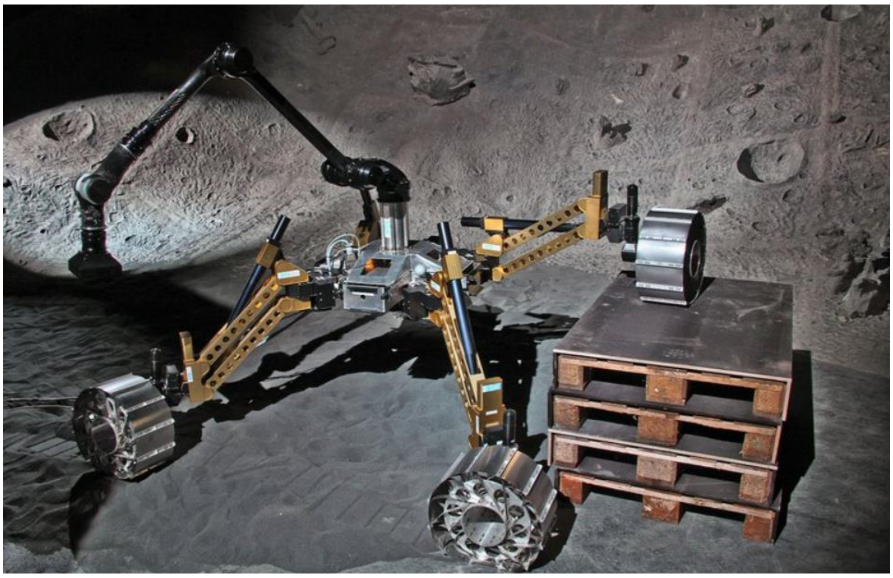

Figure 7: Sherpa Rover

The Sherpa rover is represented in Figure 7 and it is a vehicle of 160 kg of mass developed for planetary exploration equipped with an active suspension system composed of four wheeled legs of 25 kg and six active DoF each. This active system is more expensive than a passive one, however it enables the vehicle to have a better maneuverability and acquire different configurations, which would not be possible with a passive suspension system. In fact, passive suspension cannot adjust the configuration of the vehicle but only adapt it to outer forces. The problem with this system is that it may be difficult to free the vehicle if it gets stuck in mud. On the other hand, the active suspension in Sherpa is not only more flexible in adapting to the ground but can also increase traction. Furthermore, changing configuration of the four legs allow two motion modes, driving and walking, which are combined in order to present undulating locomotion capabilities.

Sherpa's active suspension is based on actuators which enable modifications of the kinematics and allow the vehicle to overcome large obstacles and to level the frame on tilted ground. When the vehicle encounters smaller impediments, active suspension is not necessary. In fact, flexible wheels made of metal and springs in the lifting actuators are sufficient to enable the vehicle to face irregularities up to one wheel diameter. In the event of wheel malfunctioning, the active suspension allows the vehicle to continue driving, by lifting off the ground the lost wheel and proceeding with the other three without altering the control system. The Sherpa rover is equipped with self-locking gears or breaks in every DoF of each leg of the suspension system, except the wheel actuators. The advantage is that no electrical energy is needed to sustain its body, preventing power consumption for position keeping. Nevertheless, the main disadvantage is that sensors cannot estimate the load of a leg in each joint because of the absence of currents. Each leg can be placed in a wide variety of positions, consequently, the vehicle can implement many configurations as well as changes in width and center of mass location. For instance, if all the Pan and Lift joints are in the initial position, the footprint has a squared shape; however, by controlling the Pan joint a long rectangular or tetragonal form can be implemented. In addition to the four legs, a manipulator is present whose role is to contribute to the locomotion, for instance as an additional leg, to intensify flexibility, but can also be used to pick up payload. The manipulator arm is also capable of sustaining the vehicle while it lifts two adjacent wheels in order to place them on a high obstacle. The active suspension allows even negative ground clearance, which is a configuration when the four wheels are raised and only the body is on the ground, which can be useful when trying to overcome impediments.

A deficiency of Sherpa's suspension is found in joints system. The first two DoF, which allow to pan and lift the leg respectively, define the position of the wheel contact point. The Lift joint is controlled by a linear pushing actuator. The following two DoF do not contribute to set the wheel location, however, they enable flipping and tilting. On hard terrain they contribute to keeping the wheel in contact with the ground. However, on soft soil, these two Dof are found to be hardly ever in use because the wheel itself is flexible and can passively adjust to the soil roughness. An additional problem with Sherpa's suspension is that even if it is equipped with an active suspension, it does not allow internal mobility, which is motion when no wheel is moving on the ground. Moreover, four of the six actuators of a leg are in close proximity of the wheel, hence preventing a compact configuration of the vehicle.

Figure 8: Sherpa TT rover

As a newer version of the Sherpa vehicle, the Sherpa TT's suspension system has an innovative design aimed at boosting flexibility, as the Figure 8 shows. The vehicle mass is 170 kg, with each leg mass of 26 kg, values that are comparable with the ones of Sherpa. The main difference between Sherpa and Sherpa TT is that in the latter the DoF which allowed the wheel to flip is removed and the one that enabled the tilting is replaced with another lifting actuator. Hence, the Sherpa TT has five of the six DoF of Sherpa and two linear actuators which constitute an additional knee joint for each leg. These actuators are positioned so that when the wheel is touching the ground, they are pulled, whereas in the Sherpa 'suspension the actuator is pushed. The consequence is that the latest version results more rigid. Another novelty is that the presence of the knee in each leg allows the wheel to be raised without interfering with motion on the x-y plane and enables internal mobility. Furthermore, it can implement a compact configuration designed originally for interplanetary transport, because of the knee enabling wider movement range.

The Sherpa TT is equipped with a sensor on every leg between the drive motor and the wheel attachment which increases the load levelling ability of the vehicle and its flexibility to adjust to different terrains, by measuring the forces and torques on the wheel. In addition, a sensor measuring temperature is present, to prevent the motors from overheating. The joints in this newer version are constituted of a set of modular actuators. From simulations and testing of the latest Sherpa version, it is found that the two actuators in Sherpa TT's suspension system need a similar amount of power. Consequently, the same motor module can be used, and this allows a reduction of gears, as well as time and costs during development [13,14].

2.4. Comparison Criteria

After the group of suspensions has been defined, several parameters are introduced to conduct the comparison among the different solution in the most objective way as possible. The selected criteria are the following:

- Cost,
- Maintenance,
- Design Complexity,
- Adaptability,
- Suspension’s Travel,
- Obstacle Avoidance,
- Actuator’s Speed-

The Cost is considered as the material cost needed to build the suspension; it is mainly based on the number, size and complexity of components. The scale is assumed from 1 to 5, being 1 the highest cost and 5 the cheapest; for instance, it is assigned the score of 1 in case of a suspension that needs a number of two very high-cost parts and a count of 5 regarding a solution that requires a total of five low-cost components.

The maintenance is defined as the need of periodic interventions to allow the correct functionalities of the suspension. The principle followed to assign the scores is to consider both the maintenance required and the concept of the possibility to execute the intervention with which each suspension is designed. The scale adopted ranges from 1, the highest maintenance needed, to 5, the least maintenance necessary. For example, it is assigned a mark of 1 to a suspension designed with in mind the possibility of regular checks and the loss of performance due to the passing of time which implies the need of recurrent intervention; the score of 5 is assigned to suspensions that are capable of work even for several years without any intervention.

The design complexity takes into account the components complexity and the needs of pre-assembled parts. This criterion is evaluated considering the number of components, actuators and assemblies required. The marks are from 1 to 5, being 1 the most complex design and 5 the easier one. For example, a score of 1 is assigned to a suspension that requires two or more complex pre-assembled parts, while 5 can be given if no preassembled components are required.

The adaptability is defined as the ability of suit different kind of soils and slopes. This parameter considers the minimum width of the rover and its steering radius. The score is ranging from 1, the lowest adaptability, to 5, the best. A mark equal to 1 is given if the rover cannot freely adjust the width occupied and takes a lot of space to execute a turn, while if a rover can reduce its width thanks to dedicated actuators and it has a narrow steering radius a score of 5 is given.

The suspension’s travel is the maximum vertical displacement of the wheel compared to the body of the rover. The scores attributed are ranging from 1, assigned to a low displacement suspension, to 5, a high displacement one. For example, 1 is given to a suspension travel that is lower than the wheel diameter, while 5 is ascribed to a travel that allows the wheel to go even higher than the center of gravity of the rover, meaning it allows a negative ground clearance.

The obstacle avoidance is considered as the ability of the rover to dodge impediments such as steps, potholes and similar. This criterion accounts for the degrees of freedom allowed by the suspension paired with its steering radius. The score varies from 1 to 5, being 1 the lower capability and 5 the greatest capacity in avoiding obstacles. For instance, 1 is assigned to a suspension that does not allow the obstacle without the intervention of the steering with also a large steering radius; a score of 5 is given to a solution that permits the obstacle avoidance thanks to its actuators and it also has a small steering radius.

The actuator’s speed is defined as the velocity of the actuators of the active suspension. This parameter takes into account the kind of actuator implemented and the cooperation among them if more are present. The mark scale ranges from 1, if the actuation is slow, to 5 if the movement is performed in a fast manner. A score of 1 is assigned if the actuation is not present, or if the degree of freedom is not directly controlled by the actuator, while a mark of 5 is given to a solution capable of controlling directly the degree of freedom, allowing also an easier control of the suspension.

Based on the afore mentioned criteria the result of the evaluation for each suspension is shown in Table 2 where the light blue highlights the best score and the red the worst, and resumed in Figure 9.

	Cost	Maintenance	Design Compl.	Adaptability	Travel	Obs.Avoid.	Act. speed
Rocker Bogie	**5**	**5**	**5**	**1**	**1**	**1**	**/**
SMA	**4**	**4**	**5**	**1**	**1**	**1**	**3**
Hylos	**4**	**4**	**4**	**3**	**3**	**3**	**3**
Athlete	**1**	**1**	**1**	**4**	**5**	**5**	**3**
Sherpa	**2**	**2**	**3**	**4**	**5**	**4**	**5**
Sherpa TT	**2**	**1**	**2**	**5**	**4**	**5**	**4**

Table 2: Evaluation of the rover's suspension based on the selected criteria

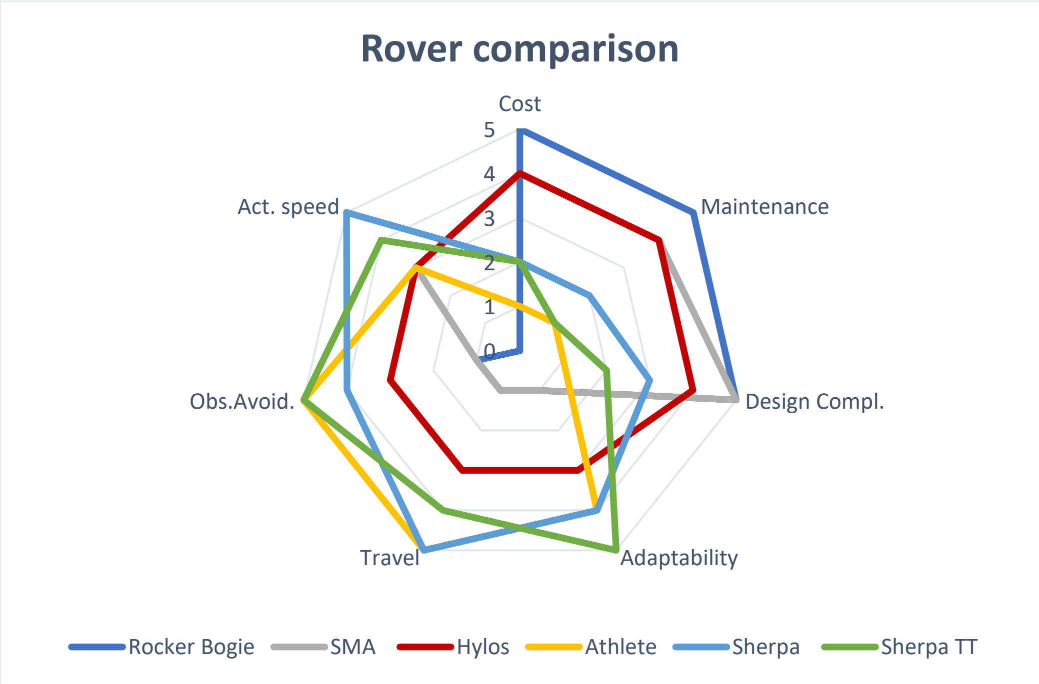

Figure 9: Rover comparison's chart

2.5. Decision Criteria

To evaluate each type of suspension, specific scores are assigned on the basis of technical characteristics, strengths and weaknesses. In this way it is possible to choose the most appropriate solution for the case studied. The seven criteria chosen and the reasons that led to their scores will then be analyzed in detail for the most interesting solutions.

COST:

- Hylos: score 4, since it is made of two arms, a linear actuator and a rotation one for the steering.
- Sherpa: score 2, because it has two arms and 6 actuators.
- Sherpa TT: score 2, because it has two arms, a joint and 6 actuators.

MAINTENANCE:

- Hylos: score 4, the linear actuator is the only component that needs check few times over usage.
- Sherpa: score 2, the six actuators need operations to ensure the correct functionalities.
- Sherpa TT: score 1, on top of what said for the Sherpa, the joint needs to be checked in order to avoid failures.

DESIGN COMPLEXITY:

- Hylos: score 4, need of assembly of 4 simple legs.
- Sherpa: score 3, need of assembly of 4 legs with average complexity.
- Sherpa TT: score 2, need of assembly of 4 complex legs.

ADAPTABILITY:

- Hylos: score 3, independent suspension allows better adaptability, but suspension travel is limited.
- Sherpa: score 4, independent suspension but minimum volume is not optimized.
- Sherpa TT: score 5, independent suspension and minimum volume are optimized.

SUSPENSION'S TRAVEL:

- Hylos: score 3, limited by the leg's length, it can be improved.
- Sherpa: score 5, it allows the negative ground clearance.
- Sherpa TT: score 4, the joint can cause a slightly inferior suspension's travel compared to Sherpa.

OBSTACOLE AVOIDANCE:

- Hylos: score 3, independent suspension allows to raise one wheel at time to avoid small obstacles without steering.
- Sherpa: score 4, avoids obstacle of big dimensions without steering.
- Sherpa TT: score 5, the two legs connected with the joint allows the most flexibility.

ACTUATOR'S SPEED:

- Hylos: score 3, each leg has its own linear actuator.
- Sherpa: score 5, 6 actuators allow a faster action.
- Sherpa TT: score 4, the joint can cause a slower action compared to Sherpa.

To arrive at the final choice, it has been decided to evaluate each suspension giving greater weight to the following aspects:

- No marks equal to 1 or 2,
- Score average higher than 3,
- At least an evaluation more than 3.

This allowed to assess which is the suspension that has an average score and consequently is the best possible choice in terms of cost, efficiency and effectiveness. The data in Table 3 show the values of arithmetic mean and weighted average for each solution analyzed.

	Rocker Bogie	SMA	Hilos	Athlete	Sherpa	Sherpa TT
Arithmetic Average	3.00	2.71	3.43	2.86	3.57	3.29
Weighted Average	2.89	2.90	3.50	2.64	3.41	3.10

Table 3: Average score for each suspension type

The difference among the two is due to the higher importance given to Cost and Design Complexity, while less importance is attributed to the Actuator’s Speed. The best Choice is the Hylos’ Suspension, scoring the highest weighted average, hence this solution is selected as guide for this study.

3. Kinematic analysis and area of reachability

3.1. Theory recall

The Hylos' Arms can be modelled as a multi-Body system composed of three main parts:

- The main body,
- The first part of the arm connecting the body to the second part,
- The second part of the arm connected to the wheel.

In order to study the kinematic and the area of reachability the convention of Denavit-Hartemberg [15] is adopted to choose the reference systems and the way they are constrained one to the other. According to such convention and starting from the base link, in this specific case the body, the links are numbered sequentially from 0 to n and the joints from 1 to n.

Joint it is assumed to be at the proximal end of link i; joint i connects link i to link i-1.

Except for the base (i=0) and the end link (i=n), the coordinate frame i (O_i-x_i y_i z_i) is attached to link i according to the following rules:

- the axis z_i is aligned with the axis of joint i, with positive direction consistent with the joint degree of freedom;
- origin O_i is located at the intersection of axis zi with the common normal to axes z_i and z_{i+1};
- the axis xi is along the common normal between axes z_i and z_{i+1} with direction from joint i to joint i+1;
- when axes z_i and z_{i+1} are parallel, the common normal between them is not uniquely defined and axis x_i can be chosen anywhere perpendicular to the two joint axes;
- when axes z_i and z_{i+1} intersect, the origin O_i is at point of intersection and axis x_i is perpendicular to the plane established by axes z_i and z_{i+1} with arbitrary direction;
- the axis y_i is defined so as to complete a right-handed frame.

The reference frame 0 is attached to the base at any convenient location as long as the axis z_0 is aligned with the first joint axis (axis z_1) and, for convenience, axis x_0 is parallel to x_1 when the degree of freedom of the first joint is null.

The reference frame n is attached to the end link n at any convenient location as long as the axis z_n is aligned with the axis of joint n and, for convenience, axis x_n is parallel to x_{n-1} when the degree of freedom of the end joint n is null.

After having defined the reference systems, the four Denavit-Hartemberg parameters can be evaluated, they are:

- α the angle required to rotate the axis z_{i-1} into alignment with the axis z_i in the right-hand direction about x_{i-1};
- a the offset distance between axes z_{i-1} and z_i measured along axis x_{i-1};
- d the distance to translate the axis x_{i-1} into incidence with the axis x_i along the positive direction of axis z_i;
- θ the angle required to rotate the axis x_{i-1} into alignment with the axis x_i in the right-hand sense about axis z_i.

For a prismatic joint i, α_{i-1}, a_{i-1} and θ_i are constant link parameters and d_i is a joint variable to measure the relative location of link i with respect to link i-1. While for a revolute joint i, α_{i-1}, a_{i-1} and di are the constant link parameters and θ_i is the joint variable to measure the relative location of link i with respect to link i-1.

After having computed the four parameters for each coordinate system it is possible to use them to obtain the transformation matrix of the successive reference system as it is shown below:

$$^{i-1}\hat{A}_i = \begin{bmatrix} \cos\theta_i & -\sin\theta_i & 0 & a_{i-1} \\ \sin\theta_i \cdot \cos\alpha_{i-1} & \cos\theta_i \cdot \cos\alpha_{i-1} & -\sin\alpha_{i-1} & -d_i \cdot \sin\alpha_{i-1} \\ \sin\theta_i \cdot \sin\alpha_{i-1} & \cos\theta_i \cdot \sin\alpha_{i-1} & \cos\alpha_{i-1} & d_i \cdot \cos\alpha_{i-1} \\ 0 & 0 & 0 & 1 \end{bmatrix}$$

3.2. Result for different solutions

Beside the layout of the Hylos rover, two other arrangements are taken into account to evaluate benefits and drawbacks. The number of joints is always two, but they are arranged in different manner, as reported in the following cases.

- Case 1 – Two Rotary joints allowing the rotation about the y axis as showed in Figure 10, while in Table 4 the Denavit-Hartemberg parameters are presented.

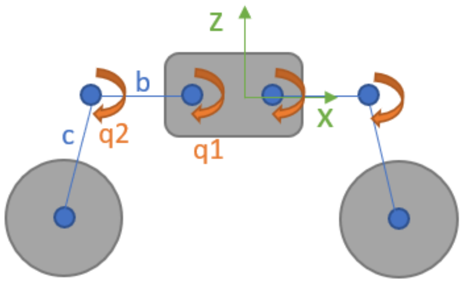

Figure 10: Case 1 scheme

	α	a	d	θ
1	0	0	0	q1
2	0	b	0	q2
3	-90	0	-c	0

Table 4: Case 1 Denavit-Hartemberg's parameters

- Case 2 – Two rotary joints: one placed on the rover body allowing the rotation about the z axle, and the other placed in between the two parts of the arm ensuring the rotation about the y axis of the rover body as showed in Figure 11, while in Table 5 the Denavit-Hartemberg parameters are presented.

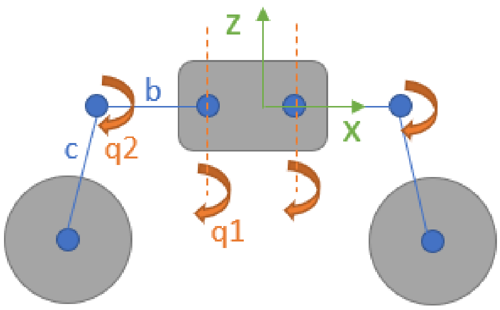

Figure 11: Case 2 scheme

	α	a	d	θ
1	0	0	0	q1
2	90	0	b	q2
3	-90	0	-c	0

Table 5: Case 2 Denhavit Hartemberg's parameters

- Case 3 – A rotary joint placed on the body that allows the rotation about the y axis and a prismatic joint allowing the elongation of the second part of the arm along its own axis as showed in Figure 12, while in Table 6 the Denavit-Hartemberg parameters are presented.

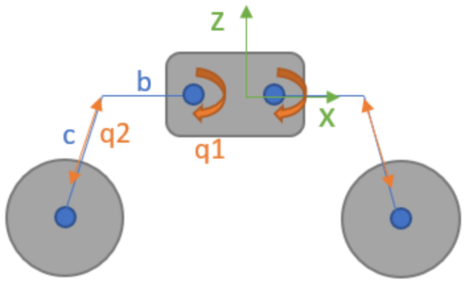

Figure 12: Case 3 scheme

	α	a	d	θ
1	0	0	0	q1
2	-90	b	q2	0
3	0	0	-c	0

Table 6: Case 3 Denavit-Hartemberg's parameters

By running MATLAB scripts specifically written (Appendices A, B, C) using the above mentioned parameters it is possible to show the kinematic of these solutions for given angles and displacement, the Figures 13, 14 and 15 show the trajectories of the arms for case 1, 2 and 3 respectively where in blue are represented the rotary joint, while in green the prismatic one. Furthermore, the green link indicates the starting configuration of the first part of the arm connecting the body to the second part, while red one indicates its finishing place; the light blue link represents the link connecting the wheel to the first part of the arm at its starting position, while the yellow one shows its final condition.

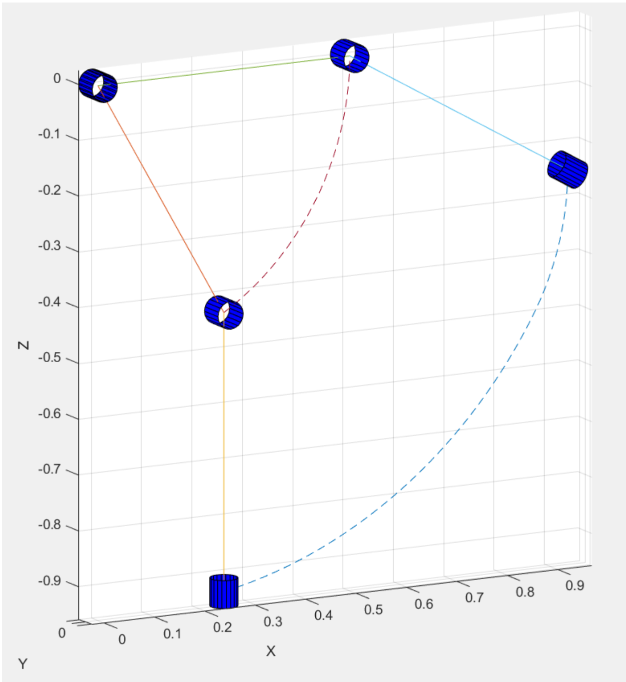

Figure 13: Case 1 trajectory

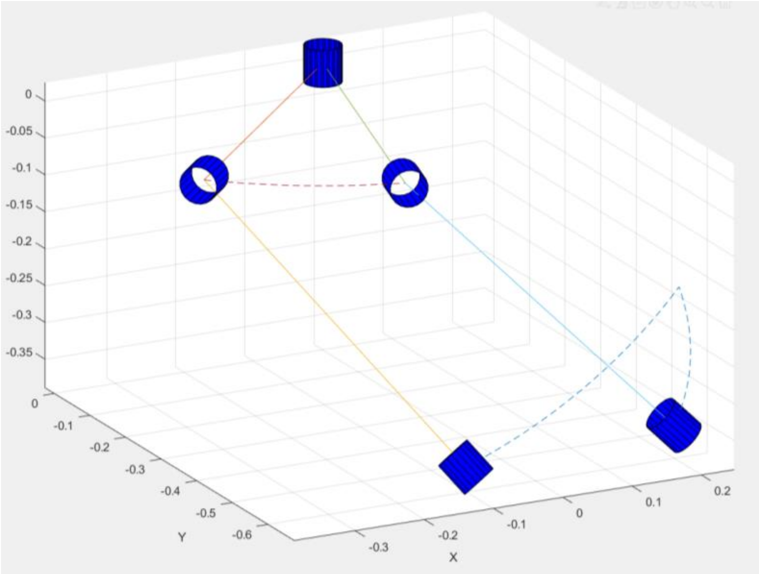

Figure 14: Case 2 trajectory

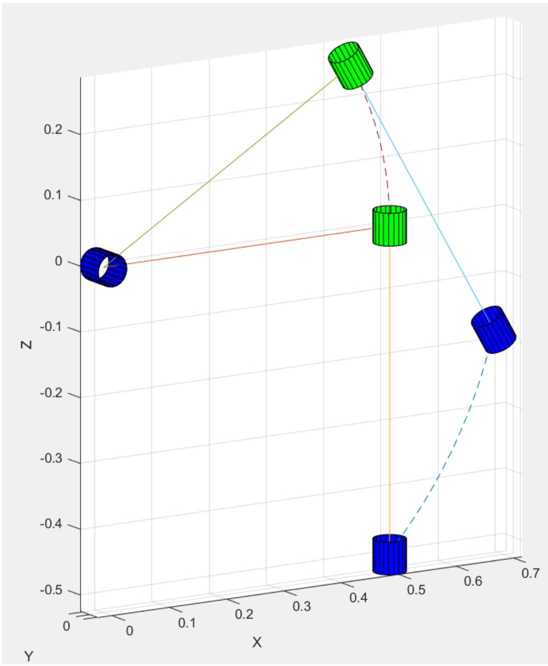

Figure 15: Case 3 trajectory

3.3. Comparison

Case 1 has the best flexibility, but it cannot move the wheel aside; furthermore, the height adjustments are performed with rotation, so a slower action is expected. Case 2 is the only one that allows the rotation along a different axle, useful for obstacle avoidance if the field is wide enough; in some configuration could cause capsize; only one rotation for height adjustment makes it the slowest in terms of ground clearance modifications. Case 3 is the fastest in performing height adjustments thanks to the linear actuator, but this choice gives the worst area of reachability and less flexibility of the three. Overall, the main downside that case 2 and 3 have, compared to case 1, is the lack of steering actuation whenever the part of the arm connected to the wheel is not perpendicular to the ground.

Considering the benefits and the drawbacks of each solution, the first case has been selected to be further developed.

4. Rover's arm modeling

4.1. Actuator dimensioning

In order to dimension the actuators' torque, it is necessary to know the total mass of the rover and the length of the arms. An iterative analysis has been performed to achieve masses and lengths that could have been sustained by stepper motors, which would have allowed the height adjustments of the rover.

Hereinafter the dimensions of principal parts of the rover are:

- Mass of the main body equal to 15 kg, not including the actuators
- Length of the first and second part of the arm equal to 280mm
- Section of part attached to the body, from now on referred as first part of the arm, equal to 50x40mm thick 5mm
- Section of the part connected to the wheel, from now on referred as second part, equal to 50x50mm thick 3mm

Regarding the material for the body, the arms and the joint components, the aluminum alloy 6063 T6 has been chosen. This material is an aluminum-magnesium-silicon alloy that has good characteristics such as sufficient tool workability in the T6 state, excellent aptitude for decorative, protective and thick anodic oxidation, high resistance to atmospheric corrosion, good resistance to marine corrosion and excellent weldability. After fixing these parameters, it is possible to compute the torque needed to raise the body of the rover from its minimum height, which is also the maximum distance of the wheel from the body, hence the most critical scenario for the actuator.

The angles that the two parts of the arm can perform have been limited as it follows: the part connected to the main body can rotate of +65° and – 65° compared to the horizontal axis as shown in Figure 16, while the part connected to the wheel can assume angle in the range between -50° and -130° compared to the horizontal axle.

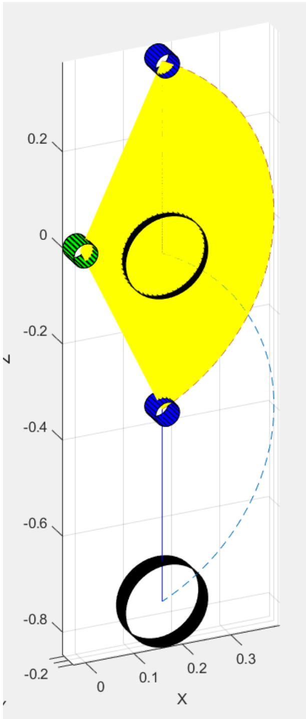

Figure 16: Area of reachability of the 1st part of the arm highlighted in yellow, while the 2nd part is kept vertical

Other constraints have been introduced regarding the rotation of the second actuator: in order to avoid unwanted interferences among components whenever the second arm rotates toward the rover's body the angle difference between the first and second part of the arm must be equal or greater than 30° (Figure 17).

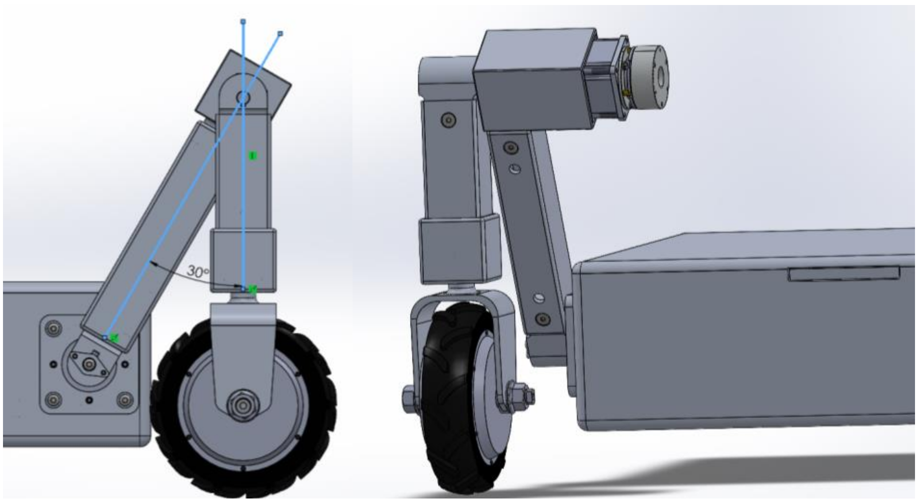

Figure 17: Rover arm configuration with 1st part at 60° and the 2nd at -90°, ensuring a 30°

Whenever the second part rotates outwards, moving the wheel far from the body, the following equation must be satisfied to ensure a minimum height of 50 mm between the bottom of the body and the ground:

$$l_1 \sin\theta_1 + l_2 \sin\vartheta_2 + r_w - d \geq h_{\min}$$

Where: l_1 and l_2 are the lengths of the arms, r_w is the radius of the wheel, d is the distance between the attachment point of the first part and the bottom of the rover and h_{min} = 50 mm is the minimum height from the ground.

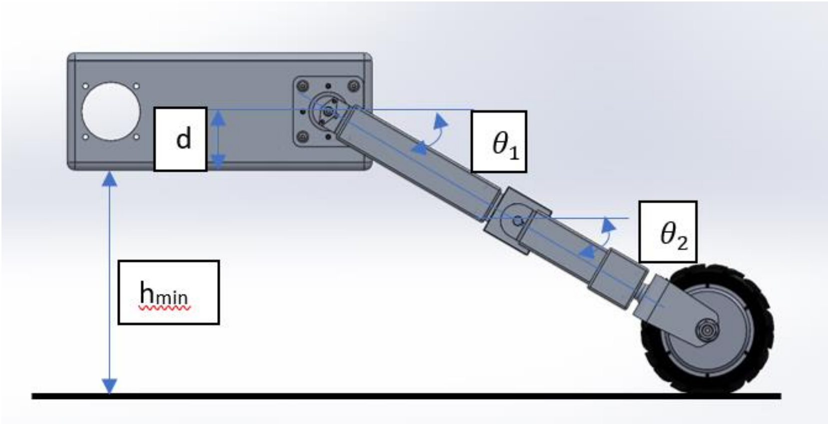

Figure 18: Parameters for the angle limit of the 2nd part of the arm

For the actuation of the rover arm the stepper motor have been chosen since they allow a precise control of the arm angles. In order to select the best solution for this specific case, the momentum generated is assumed as the product of the weight applied on the actuator by the arm assumed as the horizontal distance between actuator and the wheel ground contact patch. The torque has been computed in the most critical situation, that occurs when the wheels are the furthest from the body resulting in the longest arm. It is assumed that in order to raise the height of the rover from this position a greater torque is requested from the actuator. To achieve this condition considering the angle limitations, the first part is positioned horizontally, while the second is at -50° from the horizontal axis. Starting from this scenario, the torque needed to raise the body has been computed for two actuators of each arm: the first one will allow the first part of the arm to rotate, while the second actuator will permit the motion of the second part of the arm. To obtain the value of the momentum the sum of the weights of body, battery, motors, gearboxes and brakes is multiplied with the length of the arm. For the computation of the torque of the first actuator the second one is lock in position and the length of the arm is the sum of the length of the first part of the rover's arm plus the length of the second one multiplied by the sin(50), due to the angle limits; the torque output is equal to 46.7 Nm. The computation of the second actuator's torque is performed with the first one locked, resulting in a smaller arm and thus the momentum output is 23.1 Nm.

In order to satisfy the torque requirements mentioned above, the actuators and gearboxes from Dunkermotoren GmbH have been selected as they have the torque and mass that best suited this specific case. All the rover's arm actuations are performed by a motor and a planetary gearbox, and they are kept in place by an electromagnetic brake.

The actuators adopted for the arms are:

- Stepper motor ST 34 | 634 034 | Nema 34 34X37 (Appendix D)
- Gearbox with 2 stages PLG 75 HT (Appendix E)
- Electromagnetic brake SWB-05 (Appendix F)
- Stepper motor ST 23 | 634 023 | Nema 23 23X16 (Appendix G)
- Gearbox with 3 stages PLG 52 H (Appendix H)
- Electromagnetic brake SWB-03 (Appendix I)

The stepper motors have a step angle of 1.8° and their operating temperature window is between -20°C to +40°C. The Nema 34 is the one placed inside the rover body, and it has a rated phase current set at 8 A, capable of a holding torque of 5.50 Nm and of 5 Nm at 100 rpm. It is 96 mm long and its mass is equal to 3 kg. This motor is paired with the PLG 75HT planetary gearbox, that has a mass of 2.8 kg, 2 stages, a reduction ratio of 23.1, an efficiency of 81%, and it is 106.5 mm long and it is able to support a radial or axial load of 1000 N. The SWB-05 electromagnetic non-excited brake is applied capable of holding 4 Nm. The assembly composed by motor, gearbox and brake has a total length of 238.5 mm, a mass of 6.6 kg, a torque limited by the gearbox of 73 Nm both when the motor or the brake are used, and the top angular speed of the gearbox 'shaft is 4.33 rpm.

The Nema 23 is the one placed between the two parts of the rover arm, and it has the rated phase current set at 3 A, capable of a holding torque of 0.7 Nm and of 0.5 Nm at 400 rpm. It is 40 mm long and its mass is equal to 0.46 kg. This motor is paired with the PLG 52H planetary gearbox, that has a mass of 0.88 kg, three stages, a reduction ratio of 91.12, an efficiency of 73%, it is 80.5 mm long and it is able to support an axial load of 500 N or a radial load of 350 N. The SWB-03 electromagnetic non-excited brake is applied capable of holding 2 Nm. The assembly composed by motor, gearbox and brake has a total length of 152.5 mm, a mass of 1.54 kg, a torque limited by the gearbox of 24 Nm, both when the motor or the brake are used, and the top angular speed of the gearbox shaft is 4.38 rpm.

The motor and gearbox for the steering function are listed below:

- Stepper motor ST 17 | 634 017 | Nema 17 17X14 (Appendix J)
- Gearbox with 2 stages PLG 42 S (Appendix K)

The Nema 17 is the one placed inside the second part of the arm of the rover and it is dedicated to the steering of the wheel. Its rated phase current is set at 1.5 A, capable of a holding torque of 0.28 Nm and 0.24 Nm torque at 300 rpm, it is 36.3 mm long and its mass is equal to 0.24 kg. This motor is paired with the PLG 42S planetary gearbox, that has 2 stages, a reduction ratio of 32, an efficiency of 81%, 58.6 mm long, it has a mass of 0.37 kg and it is able to support an axial load of 150 N or radial load of 250 N. The assembly composed by motor and gearbox has a total length of 94.9 mm, a mass of 0.61 kg, a torque limited by the gearbox of 6 Nm and the top angular speed of the gearbox 'shaft is 9.37 rpm.

Assuming a total mass of 80 kg obtained by keeping in consideration the mass of the body shell, the battery, the arms, the actuators and the wheel by using a tool from the site Robotshop.com[16] the capacity of the battery and the torque required at the wheel are computed. By setting a maximum soil slope equal to 20°, a top acceleration of 0,1 m/s^2 a torque at the wheel of 6,9 Nm is required and the hub motor wheel ZLLG65ASM250-L (Double shaft) by the company ShenZhen ZhongLing Technology Co. Ltd has been selected (Appendix L). The autonomy of the rover in terms of hours is set to 4 and the top speed to 0.5 m/s as well as the afore mentioned conditions and the capacity required for only the wheel motion is equal to 27.1 Ah. Since this value does not take into account the energy needed for the actuation of the rover's arm, a lithium-ion battery with a capacity of 40 Ah has been chosen: the EVVA EV1865PACK that has a mass of 6.4kg and dimensions of 372X140X70mm (Appendix M).

All the motors used in the rover both for the arm rotation and the wheel motion and the brakes are operated at 24 V.

4.2. CAD Design

The Rover CAD is made of a main body and four arms, each with a steering wheel at their ends. Each arm is attached to the body through a keyed joint and it is made up of two parts connected through a keyed joint as well. The wheel is attached to a fork that enable the steering motion; the relative motion between arm and fork is supported by a single row angular contact ball bearing made from SKF (7203 BE-2RZP type) (Appendix N) while for the other gearbox this solution is not necessary as their radial load is sufficient for our case.

The main body is shown in Figure 19 and its dimension has been selected in order to host the the battery, the power and the signal controllers and four sub assemblies composed by motor, gearbox and brake. With regard to power control box as input there are two cables coming from the battery, while in output there will be 4 couple, positive and negative directed to each of the rover's arm while the one controlling the signal has only output cables required to control the different motors. The battery is held in place by a properly designed support with holes allowing a strap to kept it in place; a similar solution is used also to held in place the two control boxes. From the cad the support of the gearbox and the motor can be seen, their function is to avoid to rely only on the screw of the gearbox to sustain their masses. The lateral holes are dimensioned based on the PLG75HT main diameter, while the four holes are used to attached the flange. The cover is dimensioned to slot onto the main body cavity.

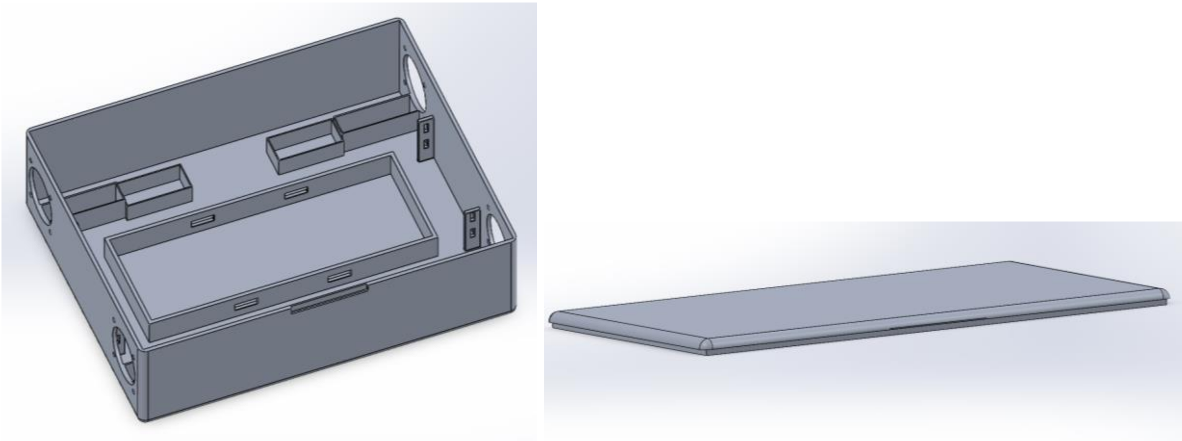

Figure 19: Rover's body

The connection between motor-gearbox assembly and the body is performed by means of flange as shown in Figure 20; the holes with a countersink for the bolt's head are the ones that kept the flange attached to the main body, while the others are used for the gearbox attachment with set screw to avoid interferences between the screw's head and the arm. The central hole, dimensioned based on the centering hole of the gearbox.

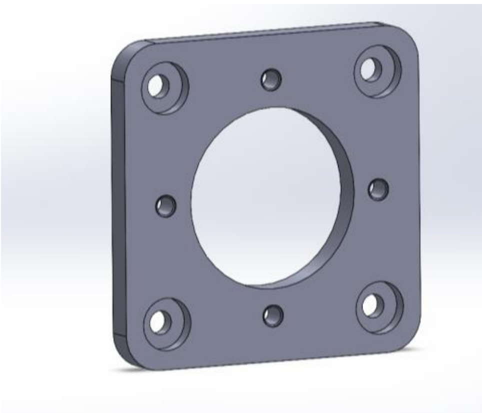

Figure 20: Flange connecting the motor with the body

Starting from the rover's body the first joint between gearbox shaft and the box section parts of the arms is made through the component shown in Figure 21, the parallelepiped extremity is dimensioned in a fashion that allows it to fit the inner part of the box section. The Box section is held in place by two M6 nuts, while to avoid this component to slip off the gearbox shaft a lock connects to the two threaded holes placed near the shaft hole.

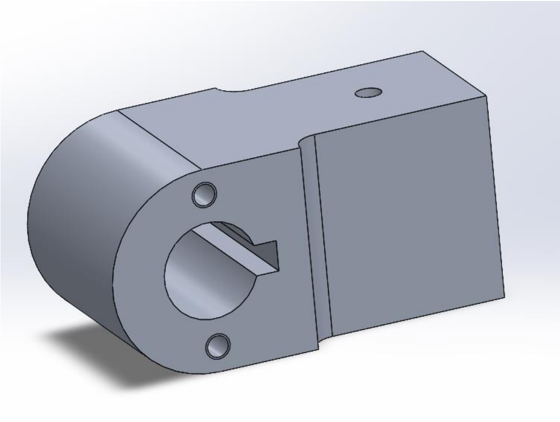

Figure 21: Joint between gearbox shaft and the box section

The first box section arm is represented in Figure 22, it has a cross section of 50X40 mm and a thickness equal to 5 mm. It has 2 holes that allow the installation guide that holds the cable needed for power and control of the other two motors and the wheel, while the other four are designed to host the four M6X12 screws to avoid the arm sliding off the joints.

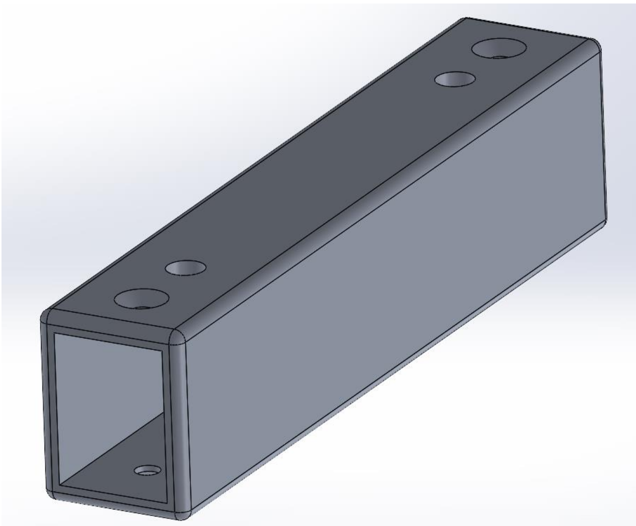

Figure 22: 1st part of the rover arm

At the other extremity of the box section arm it has been placed the motor holder, showed in Figure 23. The component's parallelepiped part is dimensioned to be hosted in the inner part of the box section, held in place by two M6X12 screws. The inner part is divided in three sections, the smaller circular hole is dimensioned based on the centering hole for the gearbox, the second circular part has increased diameter and it holds the gearbox, while the rectangular one is dimensioned to hold the motor itself, while the brake is attached to this last one by means of a flange.

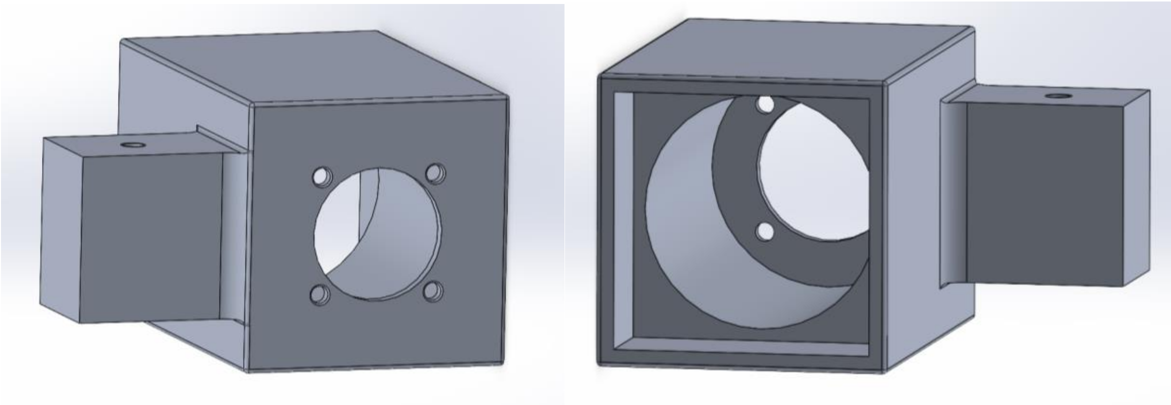

Figure 23: Component to hold the motor between the two parts of the rover arm

The second joint between the gearbox placed in between the two parts of the arm and the second box section component is performed in a similar fashion as the one used with the first actuator, and it is reported in Figure 24. The dimensions are slightly different from before in order to be compatible with the second part of the arm's specifications. Another difference is the groove made on the shaft hole designed to host a different key from the first one. An M3 threaded hole is designed to host a grub screw that connects the shaft of the PLG52H gearbox and this component to avoid it to slide axially without interference with the second part of the rover arm. On the parallelepiped faces there are two M6 threaded hole to avoid the second part of the arm to slip.

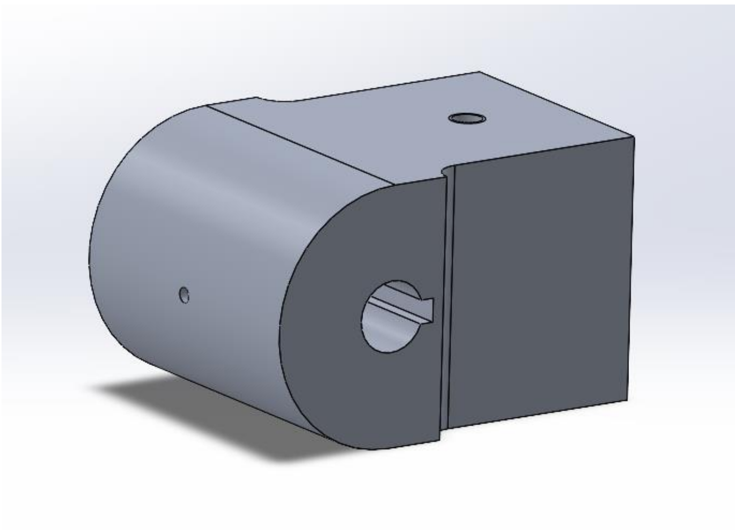

Figure 24: Connection Between PLG52H shaft and the 2nd part of the arm

The second box section part of the arm is shown in the Figure 25 and it has slightly increased dimensions for what concerns the cross section that measures 50x50 mm with a thickness of 5mm, but a reduced length of 139mm to ensure the distance of 280 mm between the shaft of the gearbox and the wheel hub. The rectangular hole on the side allows the connection of the pin of the motor dedicated to the steering motion in order to be alimented and controlled, while the two holes for the M6X12 screws are designed to fix it to the above-described component. For the second part of the rover arm no fillet is applied on the cross section faces to provide a better joint with the component that follows.

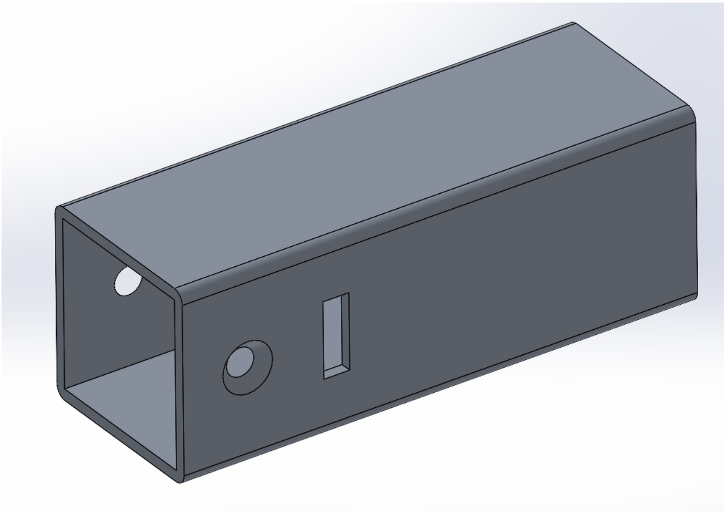

Figure 25: 2nd part of the rover arm

At the end of the second part of the arm there is a box shaped component represented in picture 26 with an open face dimensioned to allow the fitting of the external part of the second cross box arm. This component is designed to hold the gearbox and thus we can see the circular hole that acts a centering hole, which is the one with the smaller diameter, while the four threaded holes are used for the grub screws that ensure the gearbox position avoiding interference with the bearing. The circular hole with the largest diameter is designed to host the SKF angular contact bearing (Type 7203 BE-2RZP).

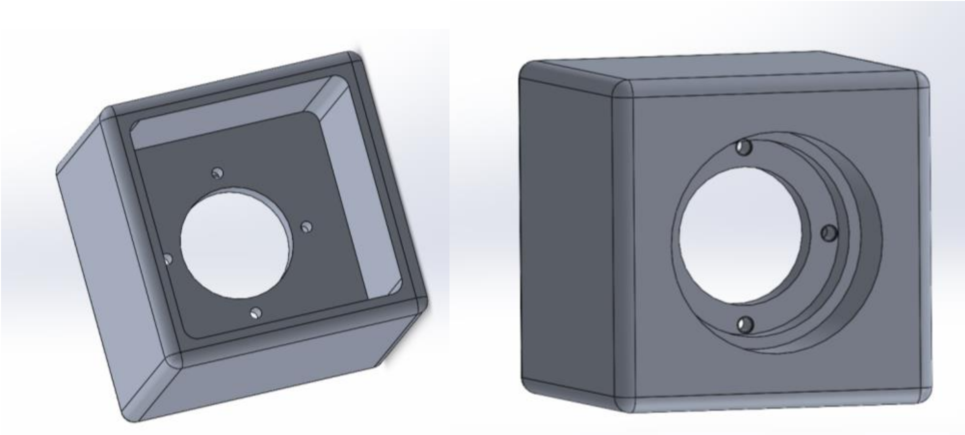

Figure 26: Connection between the 2nd part of the rover arm and the angular contact bearing

The fork is showed in Figure 27 and it is designed to be connected with the inner diameter of the bearing and also to host the shaft and the key of the gearbox inside its stem. The grooves that allow the placement of the wheel shaft are dimension to host a tab washer represented in Figure 28.

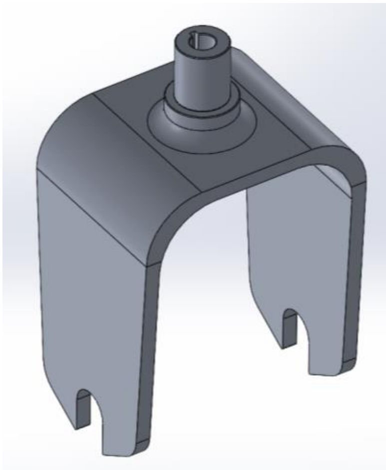

Figure 27: Rover fork

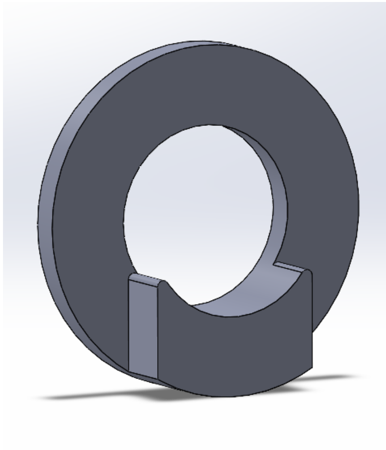

Figure 28: Fork's tab washer

The rotation of the motors is transmitted to the arms by means of a keyway and a keyseat combination and it is trasmitted only by the lateral sides fo the keys, since there is some space in the radial direction. Three different keys are used in each of the four arms and they are placed on the shaft of the gearboxes:

- Parallel key 6x6x28mm (DIN6885) is used on the shaft of the gearbox which connects the body to the first part of the arm;
- Woodruff key 4x6.5mm (DIN 6888 Series) A is used on the shaft of the gearbox that links the first with the second part of the arm;
- Woodruff key 2x3.7mm is used on the shaft of the gearbox that connects the second part of the arm with the fork.

In order to avoid that the component placed onto the shaft of the gearbox would have slide along its axial direction different solutions are adopted:

- The component placed on the shaft of the gearbox situated on the main body is held in place by a screw M6 that is fixed onto the inner thread of the shaft and by a properly designed lock plate as shown in the Figure 29. The central hole host the M6 screw, while the two at the top and bottom end are threaded M5 holes to host two grab screw ensuring the lock position.

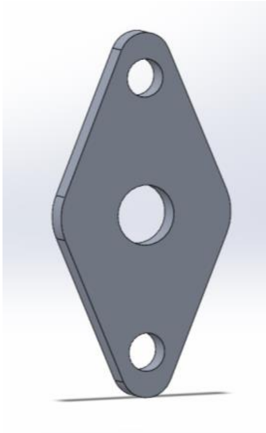

Figure 29: PLG 75H locking plate

- The component placed on the shaft of the gearbox situated between the two parts of the arm is fixed by means of a grub screw that locks its axial displacement.
- The steering mechanism is held in place by the interference with the bearing.

Two flanges are designed with proper threaded holes to allow the installation of the electromagnetic brakes represented in Figure 30.

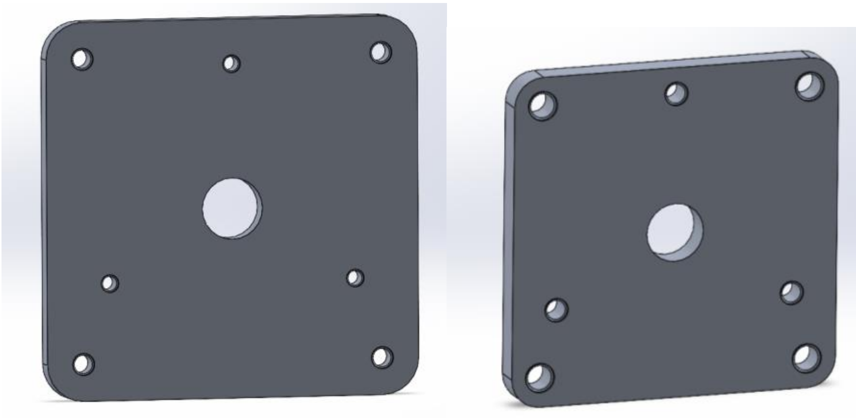

Figure 30: Left Nema 34 and right Nema 23 brake flanges

To allow the proper connection among components the following fastners are used for each of the four arms:

- 5 M6X20 hexagon bolts,
- 4 M6 nuts,
- 5 M6 washers,
- 4 M6X25 hexagon set screws,
- 6 M5X10 hexagon set screws,
- 6 M6X12 ISO10642 hexagon screws,

- 5 M3X15 hexagon set screws,
- 2 M14 tab washers,
- 2 M14 washers,
- 2 M14 flange nuts,
- 4 M5X100 hexagon screws,
- 4 M5X45 hexagon screws,
- 3 M4X8 hexagon screws,
- 3 M4X25hexagon screws.

The complete rover assembly is represented in Figure 31.

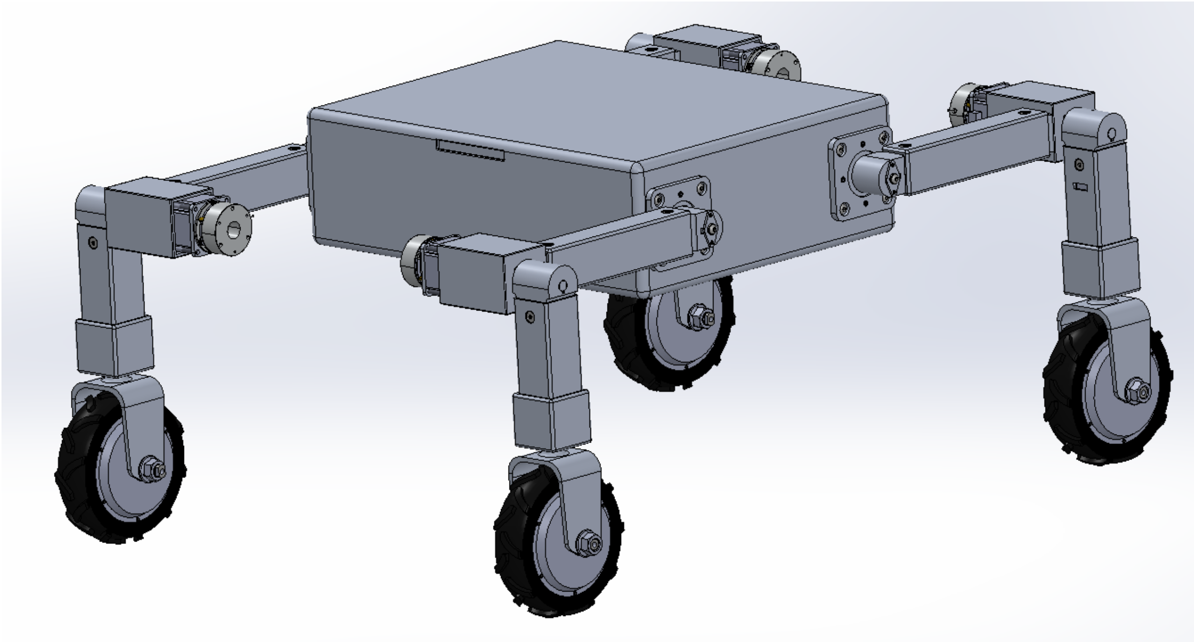

Figure 31: Complete rover assembly

In Figure 32 is showed the interior of the rover body: the blue component is the battery, while in black are shown the power and signal controllers. In the picture the motors, gearboxes and brakes are shown mounted in place.

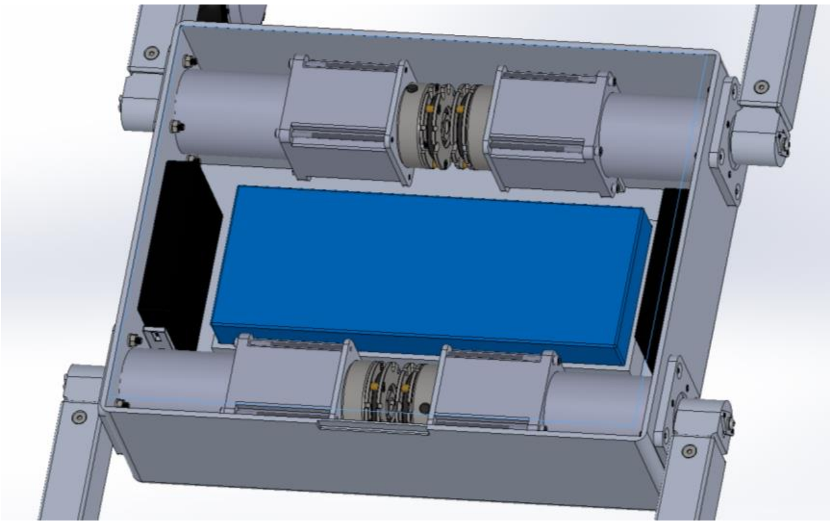

Figure 32: Rover body interiors with mounted components

In Figure 33 is represented the joint between the first part of the arm and the rover body.

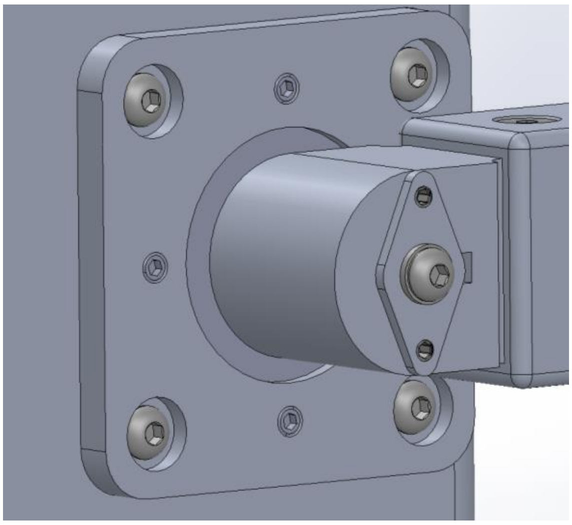

Figure 33: Rover body connection with the first part of the arm

Figure 34 shows the connection between the second part of the arm and the fork through the bearing coloured in dark grey. The wheel is kept in place with an M14 tab washer, an M14 washer and an M14 flange nut for each of its two sides.

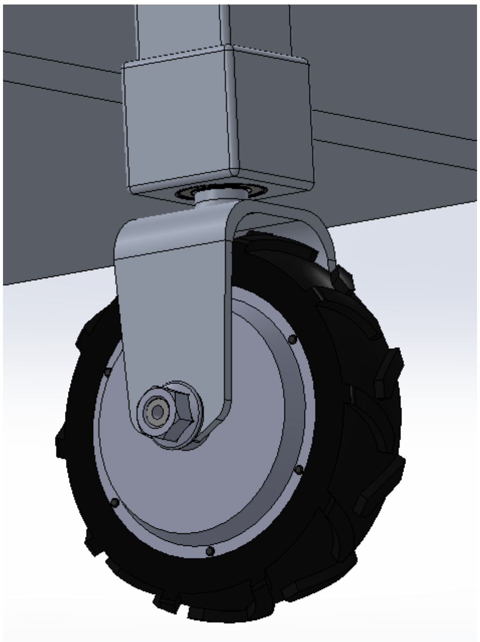

Figure 34: 2nd part of the arm connection with the wheel

4.3. Preliminary FEM analysis

The FEM analysis provides approximative solutions of the differential equations by transforming them into algebraic equations; this is possible thanks to a discretization procedure that uses mathematical models and techniques of numerical calculus. In this particular case the analysis is focused on the main body of the rover and on the two parts of the arm.

Figure 35 and 36 show the result of the analysis of the main body. The loads applied are the weight of the components, plus a force distribuited on the rover body of 100 N to simulate a payload. The constratints are applied on the shaft of the gearbox in the same way as they are when it is assembled. The peak stress are 2 orders of magnitude far from the yielding value of the material.

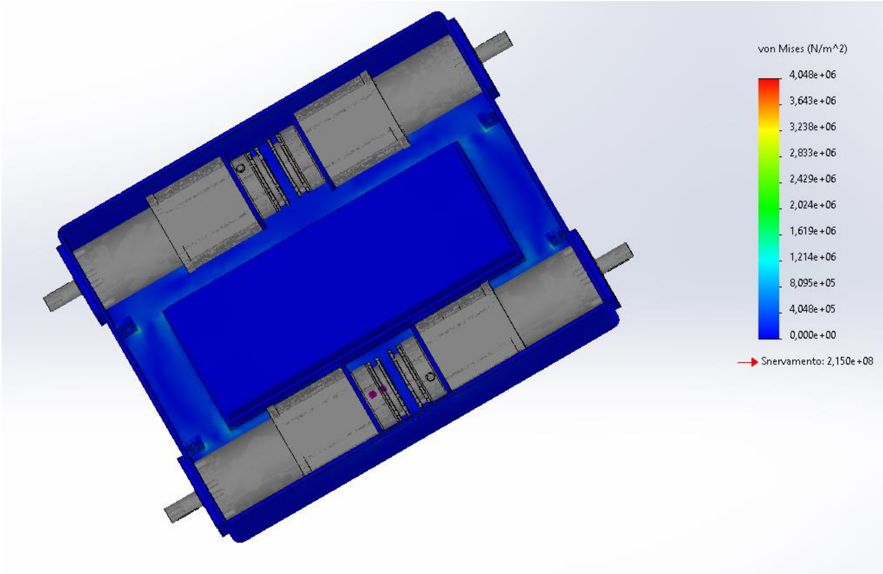

Figure 35: Rover body stress analysis

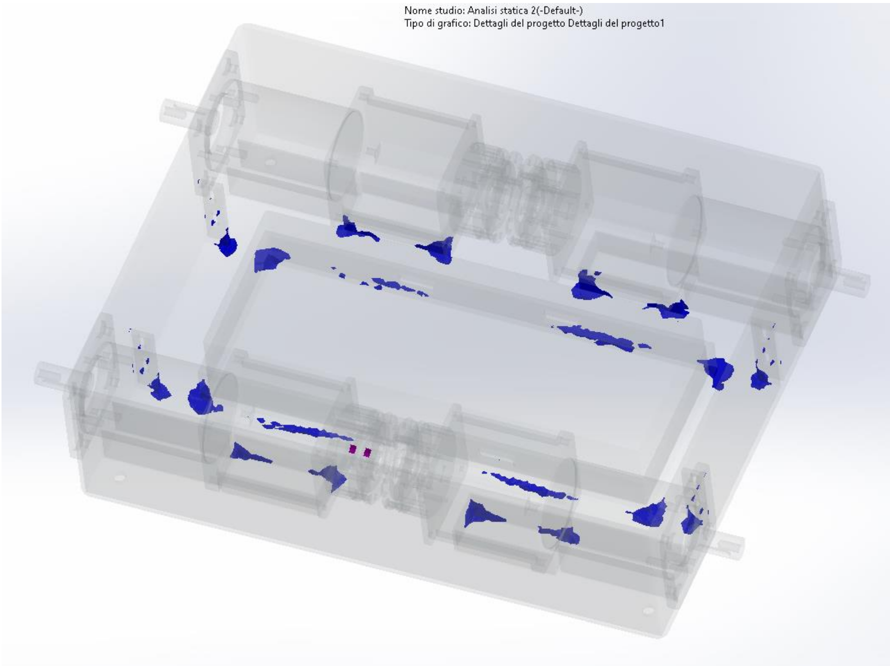

Figure 36: Most stressed areas of the body rover

In Figure 37 and 38 are pictured the results of the analysis of the first part of the rover arm. The load is a force of 250 N applied to the hole where the shaft of the first gearbox sit, simulating a total payload of approximately 25 kg on the rover equally distribuited among the four arms, with the arm positioned horizontally, id est the most critical configuration. The constratints are highlighted in green and they are applied on the shaft of the second gearbox in the same way as they are when it is assembled. The safety coefficient with this conditions is equal to 4.97 at the peak stress.

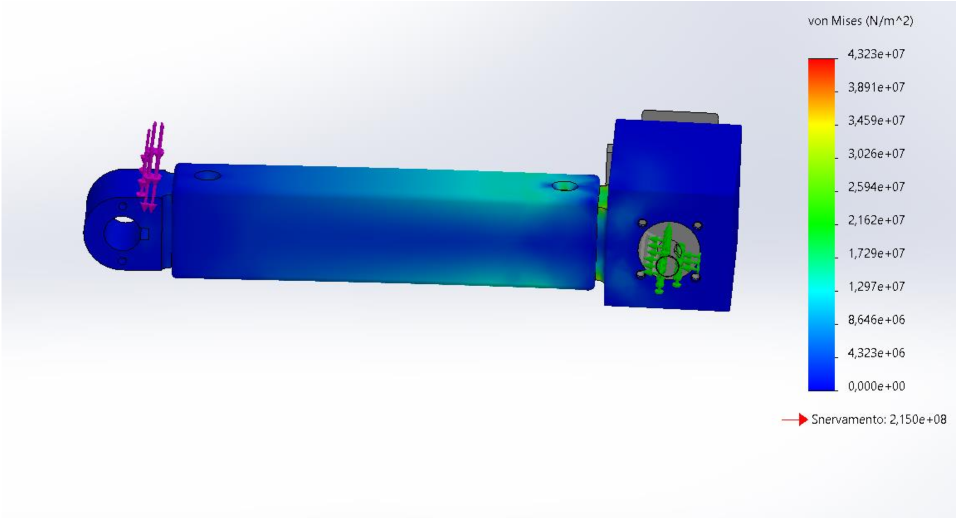

Figure 37: 1st part of the rover arm stress analysis

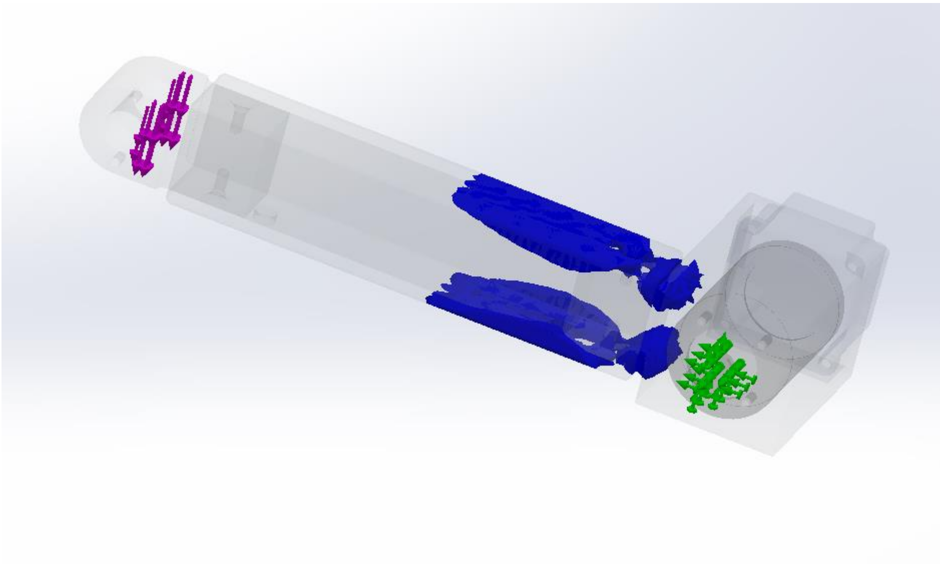

Figure 38: Most stressed areas of the first part of the rover arm

In Figure 39 and 40 the stress analysis regarding the second part of the rover arm is represented.The loads applied are the force of gravity and an external force equal to 250N applied to the hole where the shaft of the second gearbox would sit. This configuration simulate the application of a payload of approximately 25 kg. The arm is placed at -50° compared to the horizontal axis to simulate the most critical position. The safety coefficient is equal to 4 at the peak stress.

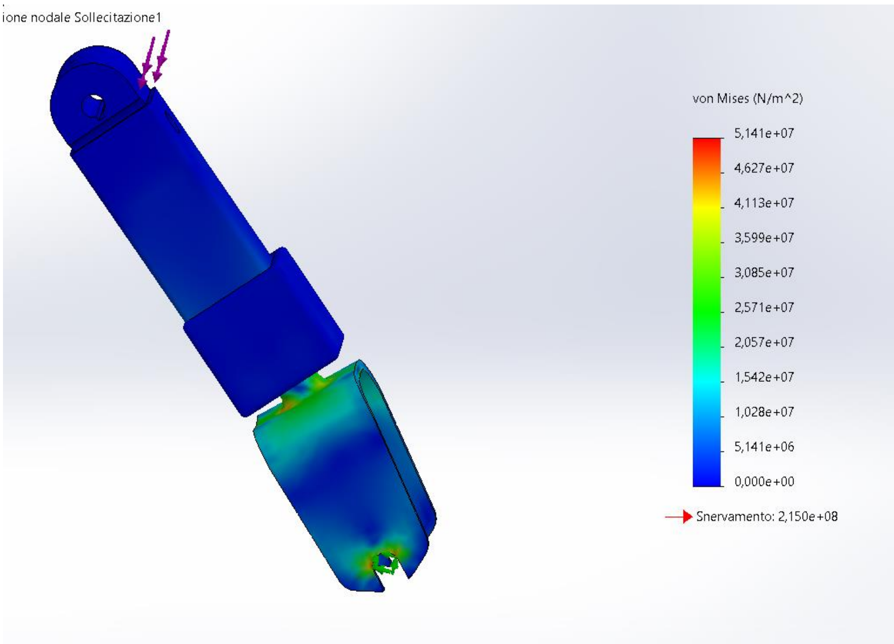

Figure 39: 2nd part of the rover arm stress analysis

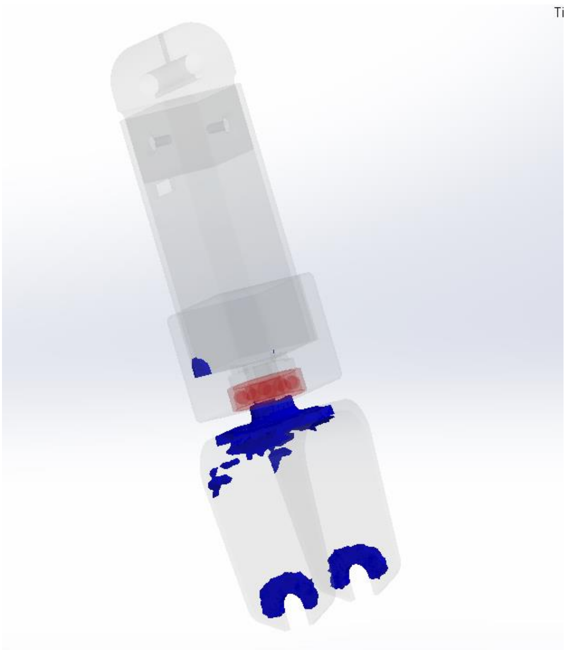

Figure 40: Most stressed area of the 2nd part of the rover arm

5. Conclusions

Starting from the analysis of different solutions adopted for rover's arm, the Hylos one has been selected as it offers the best performance overall.

The solution analysed in this thesis in based on Hylos arms, where rotations about different axis and introduction of linear actuation has been valued. Maintaining the original architecture the arms such as every one of them is divided in two parts.

A basic case has been still considered the best solution, so the focus is shifted on the rotation attuation. For the actuation a stepper motor has been chosen. After an interative process to determine mass and lenghts of the arm that could be sustained by these motors the CAD drawings have been made.

The obtained assembly shows that the chosen solution can be realized and implemented in the context of precision farming. The biggest advantage lies in the ease of realization and the ability to fit different scenarios. The simple design is an advantage both for the construction and the maintenance because it allows an easier assembly and because it requires little assistance to work properly.

The chosen rover arm model has its core strengths in terms of cost and in terms of effectiveness.

The rover has been developed by analyzing in detail its specific task, which is to scan the ground to understand its characteristics, supporting human activities. Therefore, the load it can support is quite low, in fact, as the first preliminary FEM analysis shows, its limitation are not structural, but more related to the torque that the motors can offer. As the rover is configured, the increase of payload would limit its adaptability by restraining the second part of the arm in a vertical position, but at least this part would still ensure the steering capability.

Further studies should focus on a more detailed FEM analysis to optimize the weights of the components by changing their structure, in order to verify the displacements and stress. Furthermore, the implementation of a specific control design to exploit the capability of this UGV in covering its role in the precision farming environment would permit to check constantly the fields and to spot the presence of unwanted insects or weeds obtaining the maximization of crops.

6. Bibliography

[1] https://www.agrifood.tech/precision-farming/agricoltura-di-precisione-cose-e-come-puo-aiutare-a-risolvere-le-sfide-alimentari-del-futuro/

[2] https://www.mccormick.it/us/precision-farming/

[3] https://nevonprojects.com/rough-terrain-vehicle-using-rocker-bogie-mechanism/

[4] https://mars.nasa.gov/mars2020/spacecraft/rover/wheels/

[5] https://mars.nasa.gov/msl/spacecraft/rover/wheels/

[6] https://medium.com/manual-robotics/rocker-bogie-mechanism-9e75c84a5853

[7] P. Tomaszuk, A. Łukowska, M. Rećko, K. Dzierżek and P. Straszyński, "Active wheel speed control to avoid lifting the swingarms in rocker-bogie suspension," 2019 International Young Engineers Forum (YEF-ECE), 2019, pp. 36-39, doi: 10.1109/YEF-ECE.2019.8740821.

[8] A. K. Singh, V. P. Eathakota, K. M. Krishna and A. H. Patil, "Evolution of a four wheeled active suspension rover with minimal actuation for rough terrain mobility", 2009 IEEE International Conference on Robotics and Biomimetics (ROBIO), 2009, pp. 794-799, doi: 10.1109/ROBIO.2009.5420571.

[9] Jarrault Pierre. Optimisation des capacités de franchissement des robots mobiles hybrides ”rouespattes”. Automatique / Robotique. Université Pierre et Marie Curie - Paris VI, 2013. Français. fftel-00867306f

[10] https://www.jpl.nasa.gov/videos/athlete-of-the-future

[11] J. A. Townsend, C. L. Collins, J. J. Biesiadecki, “Sliding Gait for ATHLETE Mobility”, 2014

[12] V. SunSpiral, D. Chavez-Clemente, M. Broxton, L. Keely, P. Mihelich, D. Mittman, C. Collins, “FootFall: A Ground Based Operations Toolset Enabling Walking for the ATHLETE Rover”, 2008

[13] F. Cordes, C. Oekermann, A. Babu, D. Kuehn, T. Stark and F Kirchner, “An Active Suspension System for a Planetary Rover”, 2014

[14] F. Cordes, “Design and Experimental Evaluation of a Hybrid Wheeled-Leg Exploration Rover in the Context of Multi-Robot Systems”, 2018

[15] Stefano Pastorelli, Andrea Trivella. 2019. “Numerical Modelling and Simulation”, lecture notes. Politecnico di Torino, delivered October 2019.

[16] https://www.robotshop.com/community/blog/show/drive-motor-sizing-tool

7. Appendix

Appendix A – Matlab Script for Case 1 Trajectory

```
clc
close all
clear all

load trajectory.mat;

%From Deg to Rad
q1vec=q1vec*pi/180;
q2vec=q2vec*pi/180;
q3vec=q3vec*pi/180;

%% Initial and final conditions

%Initial condition
%Joint_1
alfa1=(pi/2);
a1=0;
d1=0;
teta1=q1vec(1,1);
A10o=denhar_en01(alfa1,a1,d1,teta1);

figure(1)
plot3(A10o(1,4),A10o(2,4),A10o(3,4)); hold on
joint_rev_01(0.025,0.05,20,A10o,'blu')

%Joint_2
alfa2=0;
a2=0.5;
d2=0;
teta2=(pi/2)+q2vec(1,1);
A21o=denhar_en01(alfa2,a2,d2,teta2);
A20o=A10o*A21o;

plot3([A10o(1,4) A20o(1,4)],[A10o(2,4) A20o(2,4)],[A10o(3,4) A20o(3,4)]); hold on
joint_rev_01(0.025,0.05,20,A20o,'blu')

%Joint3
alfa3=-(pi/2);
a3=0;
d3=-0.5;
teta3=-(pi/2)+q3vec(1,1);
A32o=denhar_en01(alfa3,a3,d3,teta3);
A30o=A20o*A32o;
plot3([A20o(1,4) A30o(1,4)],[A20o(2,4) A30o(2,4)],[A20o(3,4) A30o(3,4)]); hold on
joint_rev_01(0.025,0.05,20,A30o,'blu')
axis equal

%Final condition
%Joint_1
alfa1=(pi/2);
a1=0;
```

```
d1=0;
teta1=q1vec(1,1001);
A10o=denhar_en01(alfa1,a1,d1,teta1);

plot3(A10o(1,4),A10o(2,4),A10o(3,4)); hold on
joint_rev_01(0.025,0.05,20,A10o,'blu')

%Joint_2
alfa2=0;
a2=0.5;
d2=0;
teta2=(pi/2)+q2vec(1,1001);
A21o=denhar_en01(alfa2,a2,d2,teta2);
A20o=A10o*A21o;

plot3([A10o(1,4) A20o(1,4)],[A10o(2,4) A20o(2,4)],[A10o(3,4) A20o(3,4)]); hold on
joint_rev_01(0.025,0.05,20,A20o,'blu')

%Joint_3
alfa3=-(pi/2);
a3=0;
d3=-0.5;
teta3=-(pi/2)+q3vec(1,1001);
A32o=denhar_en01(alfa3,a3,d3,teta3);
A30o=A20o*A32o;

plot3([A20o(1,4) A30o(1,4)],[A20o(2,4) A30o(2,4)],[A20o(3,4) A30o(3,4)]); hold on
joint_rev_01(0.025,0.05,20,A30o,'blu')
axis equal



%% Trajectories

for i=1:length(timevec)
    %Joint_1
    alfa1=(pi/2);
    a1=0;
    d1=0;
    teta1=q1vec(1,i);
    A10o=denhar_en01(alfa1,a1,d1,teta1);

    %Joint_2
    alfa2=0;
    a2=0.5;
    d2=0;
    teta2=(pi/2)+q2vec(1,i);
    A21o=denhar_en01(alfa2,a2,d2,teta2);
    A20o=A10o*A21o;

    %Joint_3
    alfa3=-(pi/2);
    a3=0;
    d3=-0.5;
    teta3=-(pi/2)+q3vec(1,i);
    A32o=denhar_en01(alfa3,a3,d3,teta3);
    A30o=A20o*A32o;
```

```
    pCP_traiet(:,i)=A20o(1:3,4);
    pEE_traiet(:,i)=A30o(1:3,4);


end

%% Trajectory plot
plot3(pCP_traiet(1,:), pCP_traiet(2,:), pCP_traiet(3,:),'--')
plot3(pEE_traiet(1,:), pEE_traiet(2,:), pEE_traiet(3,:),'--')
```

Appendix B – Matlab Script for Case 2 Trajectory

```
clc
close all
clear all

load trajectory1.mat;

%From Deg to Rad
q1vec=q1vec*pi/180;
q2vec=q2vec*pi/180;
q3vec=q3vec*pi/180;

%% Initial and final conditions

%Initial condition
%Joint_1
alfa1=0;
a1=0;
d1=0;
teta1=q1vec(1,1);
A10o=denhar_en01(alfa1,a1,d1,teta1);

figure(1)

plot3(A10o(1,4),A10o(2,4),A10o(3,4)); hold on
joint_rev_01(0.025,0.05,20,A10o,'blu')

%Joint_2
alfa2=(pi/2);
a2=0;
d2=0.5;
teta2=(pi/2)+q2vec(1,1);
A21o=denhar_en01(alfa2,a2,d2,teta2);
A20o=A10o*A21o;

plot3([A10o(1,4) A20o(1,4)],[A10o(2,4) A20o(2,4)],[A10o(3,4) A20o(3,4)]); hold on
joint_rev_01(0.025,0.05,20,A20o,'blu')

%Joint3
alfa3=-(pi/2);
a3=0;
d3=-0.5;
teta3=-(pi/2)+q3vec(1,1);
A32o=denhar_en01(alfa3,a3,d3,teta3);
A30o=A20o*A32o;

plot3([A20o(1,4) A30o(1,4)],[A20o(2,4) A30o(2,4)],[A20o(3,4) A30o(3,4)]); hold on
joint_rev_01(0.025,0.05,20,A30o,'blu')
axis equal

%Final condition
%Joint_1
alfa1=0;
a1=0;
d1=0;
```

```
teta1=q1vec(1,1001);
A10o=denhar_en01(alfa1,a1,d1,teta1);

plot3(A10o(1,4),A10o(2,4),A10o(3,4)); hold on
joint_rev_01(0.025,0.05,20,A10o,'blu')

%Joint_2
alfa2=(pi/2);
a2=0;
d2=0.5;
teta2=(pi/2)+q2vec(1,1001);
A21o=denhar_en01(alfa2,a2,d2,teta2);
A20o=A10o*A21o;

plot3([A10o(1,4) A20o(1,4)],[A10o(2,4) A20o(2,4)],[A10o(3,4) A20o(3,4)]); hold on
joint_rev_01(0.025,0.05,20,A20o,'blu')

%Joint_3
alfa3=-(pi/2);
a3=0;
d3=-0.5;
teta3=-(pi/2)+q3vec(1,1001);
A32o=denhar_en01(alfa3,a3,d3,teta3);
A30o=A20o*A32o;

plot3([A20o(1,4) A30o(1,4)],[A20o(2,4) A30o(2,4)],[A20o(3,4) A30o(3,4)]); hold on
joint_rev_01(0.025,0.05,20,A30o,'blu')
axis equal


%% Trajectories

for i=1:length(timevec)
    %Joint_1
    alfa1=0;
    a1=0;
    d1=0;
    teta1=q1vec(1,i);
    A10o=denhar_en01(alfa1,a1,d1,teta1);

    %Joint_2
    alfa2=(pi/2);
    a2=0;
    d2=0.5;
    teta2=(pi/2)+q2vec(1,i);
    A21o=denhar_en01(alfa2,a2,d2,teta2);
    A20o=A10o*A21o;

    %Joint_3
    alfa3=-(pi/2);
    a3=0;
    d3=-0.5;
    teta3=-(pi/2)+q3vec(1,i);
    A32o=denhar_en01(alfa3,a3,d3,teta3);
    A30o=A20o*A32o;

    pCP_traiet(:,i)=A20o(1:3,4);
    pEE_traiet(:,i)=A30o(1:3,4);
```

```
end

%% Trajectory plot
plot3(pCP_traiet(1,:), pCP_traiet(2,:), pCP_traiet(3,:),'--')
plot3(pEE_traiet(1,:), pEE_traiet(2,:), pEE_traiet(3,:),'--')
grid on
```

Appendix C – Matlab Script for Case 3 Trajectory

```
clc
close all
clear all

load trajectory2.mat;

%From Deg to Rad
q1vec=q1vec*pi/180;
q2vec=q2vec*pi/180;
q3vec=q3vec*pi/180;

%% Initial and final conditions

%Initial condition
%Joint_1
alfa1=(pi/2);
a1=0;
d1=0;
teta1=q1vec(1,1);
A10o=denhar_en01(alfa1,a1,d1,teta1);

figure(1)

plot3(A10o(1,4),A10o(2,4),A10o(3,4)); hold on
joint_rev_01(0.025,0.05,20,A10o,'blu')

%Joint_2
alfa2=-(pi/2);
a2=0.5;
d2=q2vec(1,1);
teta2=0;
A21o=denhar_en01(alfa2,a2,d2,teta2);
A20o=A10o*A21o;

plot3([A10o(1,4) A20o(1,4)],[A10o(2,4) A20o(2,4)],[A10o(3,4) A20o(3,4)]); hold on
joint_rev_01(0.025,0.05,20,A20o,'green')

%Joint3
alfa3=0;
a3=0;
d3=-0.5;
teta3=q3vec(1,1);
A32o=denhar_en01(alfa3,a3,d3,teta3);
A30o=A20o*A32o;

plot3([A20o(1,4) A30o(1,4)],[A20o(2,4) A30o(2,4)],[A20o(3,4) A30o(3,4)]); hold on
joint_rev_01(0.025,0.05,20,A30o,'blu')
axis equal

%Final condition
%Joint_1
alfa1=(pi/2);
a1=0;
d1=0;
```

```
teta1=q1vec(1,1001);
A10o=denhar_en01(alfa1,a1,d1,teta1);

plot3(A10o(1,4),A10o(2,4),A10o(3,4)); hold on
joint_rev_01(0.025,0.05,20,A10o,'blu')

%Joint_2
alfa2=-(pi/2);
a2=0.5;
d2=q2vec(1,1001);
teta2=0;
A21o=denhar_en01(alfa2,a2,d2,teta2);
A20o=A10o*A21o;

plot3([A10o(1,4) A20o(1,4)],[A10o(2,4) A20o(2,4)],[A10o(3,4) A20o(3,4)]); hold on
joint_rev_01(0.025,0.05,20,A20o,'green')

%Joint_3
alfa3=0;
a3=0;
d3=-0.5;
teta3=q3vec(1,1001);
A32o=denhar_en01(alfa3,a3,d3,teta3);
A30o=A20o*A32o;

plot3([A20o(1,4) A30o(1,4)],[A20o(2,4) A30o(2,4)],[A20o(3,4) A30o(3,4)]); hold on
joint_rev_01(0.025,0.05,20,A30o,'blu')
axis equal


%% Trajectories

for i=1:length(timevec)
    %Joint_1
    alfa1=(pi/2);
    a1=0;
    d1=0;
    teta1=q1vec(1,i);
    A10o=denhar_en01(alfa1,a1,d1,teta1);

    %Joint_2
    alfa2=-(pi/2);
    a2=0.5;
    d2=q2vec(1,i);
    teta2=0;
    A21o=denhar_en01(alfa2,a2,d2,teta2);
    A20o=A10o*A21o;

    %Joint_3
    alfa3=0;
    a3=0;
    d3=-0.5;
    teta3=q3vec(1,i);
    A32o=denhar_en01(alfa3,a3,d3,teta3);
    A30o=A20o*A32o;

    pCP_traiet(:,i)=A20o(1:3,4);
    pEE_traiet(:,i)=A30o(1:3,4);
```

```
end

%% Trajectory plot
plot3(pCP_traiet(1,:), pCP_traiet(2,:), pCP_traiet(3,:),'--')
plot3(pEE_traiet(1,:), pEE_traiet(2,:), pEE_traiet(3,:),'--')
grid on
```

Appendix D – Dunkermotoren Stepper motor ST 34 | 634 034 | Nema 34 34X37

ST 34 | 634 034 | *Nema 34 stepper motor*

- 86 mm square Nema 34
- High grade Neodymium magnets
- 1.8° step angle (+/-5%)
- customized solutions available on demand
- Operating temperatures -20°C to +40°C
- Sinusoidal back EMF optimized for microstep operation and hi holding torque
- Insulation Class 130 (B)

Data		34x37	34x37	34x37	34x48	34x48	34x48	34x55	34x55	34x55	34x62
Rated phase current	A	3,00	5,50	8,00	3,00	5,50	8,00	3,00	5,50	8,00	8,00
Phase resistance	Ohm	1,24	0,42	0,2	1,5	0,465	0,215	1,7	0,55	0,29	0,33
Phase Inductance	mH	12	3,6	1,65	12,96	4	1,85	20	5,60	2,6	3,57
Holding torque Bipolar	Ncm	520	550	550	700	700	700	1000	1000	1000	1200
Detent torque	Ncm	22	27	24	31	33	32	32	33	34	51
Rotor inertia	gcm²	3460	3460	3460	3870	3870	3870	4900	4900	4900	8269
Max voltage	VDC	160	160	160	160	160	160	160	160	160	160
Weight	Kg	3,00	3,00	3,00	4,00	4,00	4,00	4,60	4,60	4,60	5,40

all data measured with standard cables 500 mm at 25°C

Modular System

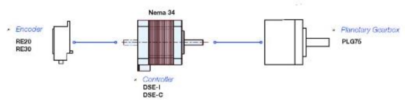

52 | Visit www.ametekmae.com for further product information

ST 34 | 634 034 | *Nema 34 stepper motor*

MAE®

Dimensions in mm

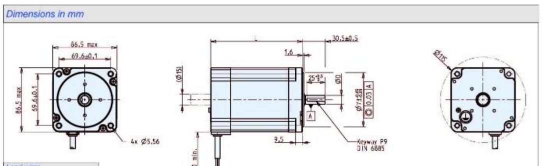

Lead wires	
Colour	Function
White	phase A+
Yellow	phase A-
Red	phase B+
Blue	phase B-

Motor	L	D ø	Keyway
34X37	96 +/-0.6	12	4x4 P9
34X48	124 +/-0.6	12	4x4 P9
34X55	141.5 +/-0.6	12	4x4 P9
34X62	158.5 +/-0.6	16	5x5 P9

Characteristic diagram

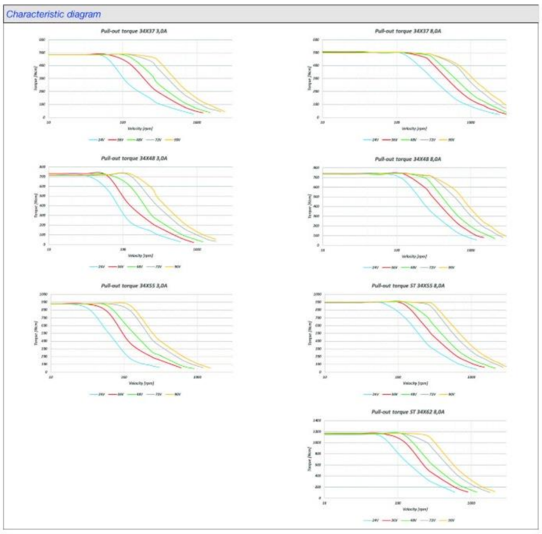

Visit www.ametekmae.com for further product information

Appendix E – Dunkermotoren Gearbox with 2 stages PLG 75 HT

PLG 75 HT

- *Industry compatible high torque planetary gearbox*
- *Protection class IP 65 standard (excluding output shaft, in combination with BG 66 or BG 75 **dCore**/ **dMove**/ **dPro**)*
- *High efficiency*
- *Output shaft with double ball bearings*

- Industrietaugliches, drehmomentstarkes Planetengetriebe
- Schutzklasse IP 65 Standard (ausgenommen Abtriebswellendichtung, in Kombination mit BG 66 oder BG 75 **dCore**/ **dMove**/ **dPro**)
- Hoher Wirkungsgrad
- Ausgangswelle doppelt kugelgelagert

Lifetime lubrication | *Food grade lubrication* | *Low temperature* | *High efficiency* | *High torque* | *Special surface available* | *Protection class (up to)* | *Vibration resistance*

Data/ Technische Daten | PLG 75 HT - *Ring gear made of steel*/ Hohlrad aus Stahl													
Reduction ratio/ Untersetzungsverhältnis	-	4	5.5	7	10	13.65	16.8	23.1	27.5	29.4	35	42	50
Efficiency/ Wirkungsgrad	%	90				81							
Number of stages/ Stufenzahl	-	1				2							
Continuous torque/ Dauerdrehmoment	Nm	25				40	73						
Acceleration torque */ Beschleunigungsmoment *	Nm	50				80	130						
Emergency stop torque/ Not-Aus Drehmoment	Nm	60		75		120	175						
Operating mode/ Betriebsart	-	S1 / S8											
Max. backlash/ Max. Verdrehspiel	arcmin	39	42	43	46	34	35	36	36	36	36	37	37
Weight of gearbox/ Getriebegewicht	kg	1.7				2.8							
Axial load/ radial load (middle of key)/ Axiallast/ Radiallast (Mitte Feder)	N	1000 / 1000				1000 / 1000							

Data/ Technische Daten | PLG 75 HT - *Ring gear made of steel*/ Hohlrad aus Stahl										
Reduction ratio/ Untersetzungsverhältnis	-	70.56	84	100	115.5	147	175	210	250	350
Efficiency/ Wirkungsgrad	%	73								
Number of stages/ Stufenzahl	-	3								
Continuous torque/ Dauerdrehmoment	Nm	90								
Acceleration torque */ Beschleunigungsmoment *	Nm	130								
Operating mode/ Betriebsart	-	S1 / S8								
Emergency stop torque/ Not-Aus Drehmoment	Nm	300								
Max. backlash/ Max. Verdrehspiel	arcmin	34	34	34	35	35	35	35	35	34
Weight of gearbox/ Getriebegewicht	kg	3.9								
Axial load/ radial load (middle of key)/ Axiallast/ Radiallast (Mitte Feder)	N	1000 / 1000								

* *Acceleration torque for max. 1 second*/ * Beschleunigungsmoment für max. 1 Sekunde

210 | *Visit www.dunkermotoren.com for further product information*/ Besuchen Sie www.dunkermotoren.de für weitere Produktinformationen

PLG 75 HT

dunkermotoren

Dimensions in mm/ Maßzeichnung in mm

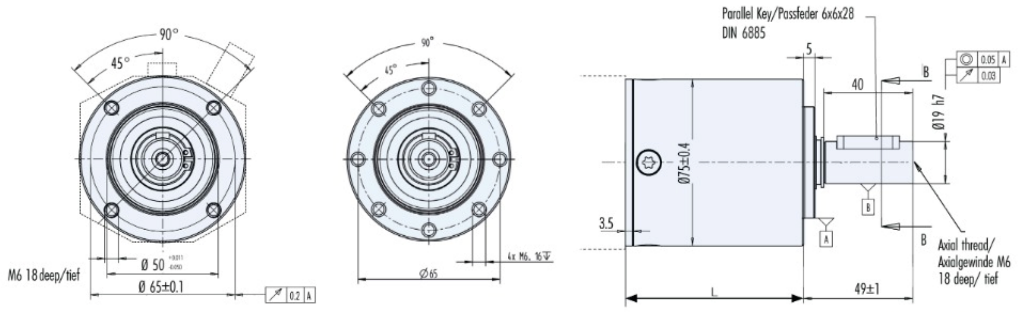

1- und 2-stufige Variante mit 4 Gewindebohrungen/
1- and 2-stage variant with 4 threaded holes

3-stufige Variante mit 8 Gewindebohrungen/
3-stage version with 8 threaded holes

Length/ Länge L mm	
1-stufig/ stage	80.2
2-stufig/ stage	106.5
3-stufig/ stage	133.7

Gearboxes

Preferred series/ Vorzugsreihe *Standard product*/ Standardprodukt *On request*/ auf Anfrage *See notes page 8*/ Hinweise siehe S. 8

Appendix F – Electromagnetic brake SWB-05

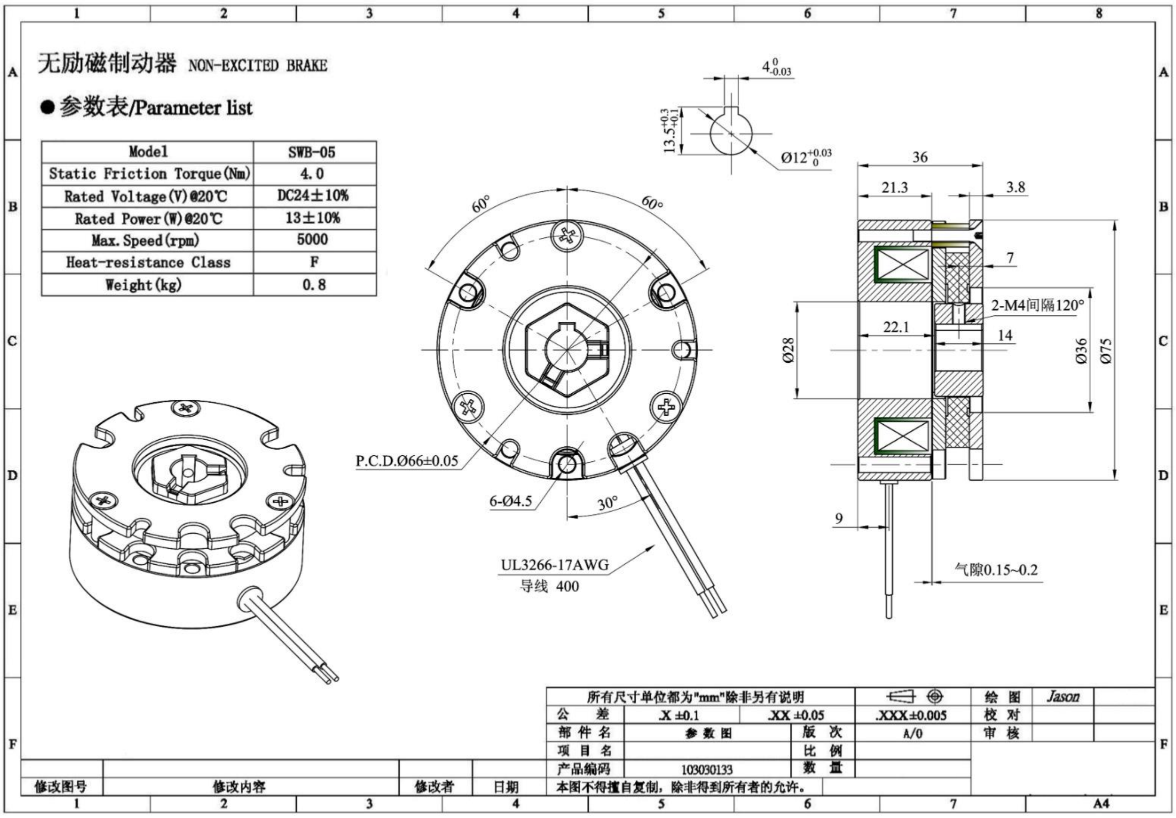

Appendix G – Dunkermotoren Stepper motor ST 23 | 634 023 | Nema 23 23X16

ST 23 | 634 023 | *Nema 23 stepper motor*

- 57 mm square Nema 23
- Hi grade Neodymium magnets
- 1.8° step angle (+/-5%)
- customized solutions available on demand
- Operating temperatures -20°C to +40°C
- Sinusoidal back EMF optimized for microstep operation and hi holding torque
- Insulation Class 130 (B)

Data		23x16	23x16	23x16	23x21	23x21	23x21	23x31	23x31	23x31	23x31
Rated phase current	A	1	2	3	1	2	3	1	2	3	4
Phase resistance	Ohm	3,67	0,98	0,42	5,14	1,33	0,61	6,26	1,57	0,69	0,43
Phase Inductance	mH	13,51	3,21	1,58	20,75	5,67	2,3	22,35	5,77	2,7	1,66
Holding torque Bipolar	Ncm	70	70	70	140	140	140	200	200	200	210
Detent torque	Ncm	3	3	3	5	5	6	8	7	7	7
Rotor inertia	gcm^2	77	77	77	209	209	209	335	335	335	335
Max voltage	VDC	80	80	80	80	80	80	80	80	80	80
Weigth	Kg	0,46	0,46	0,46	0,7	0,7	0,7	1,05	1,05	1,05	1,05

all data measured with standard cables 300 mm at 25°C

Modular System

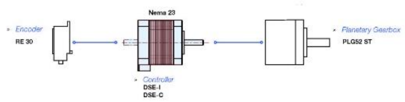

ST 23 | 634 023 | *Nema 23 stepper motor*

Dimensions in mm

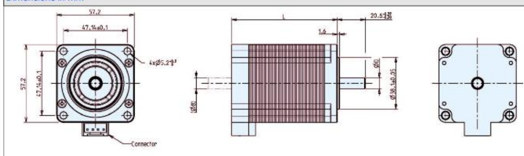

- Shaft D cut options: 5.8X15 mm or 7.5X15mm

Motor	L	D ø
23X16	40±0,6	6,35
23X21	55±0,6	6,35
23X31	78±0,6	8

Characteristic diagram

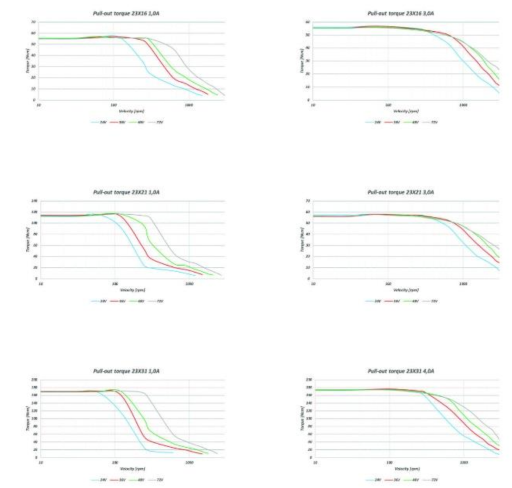

Appendix H – Dunkermotoren Gearbox with 3 stages PLG 52 H

PLG 52 H

- *High efficiency*
- *Quiet operation due to helical gears in 1st stage, 2nd and 3rd stage have straight toothing*

- Hoher Wirkungsgrad
- Für hohe Laufruhe ist erste Getriebestufe schrägverzahnt ausgeführt, 2. und 3. Getriebestufe geradeverzahnt

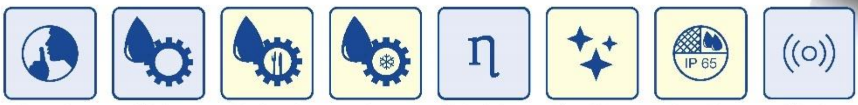

Data/ Technische Daten | PLG 52 H - Low noise/ Hohe Laufruhe																		
Reduction ratio/ Untersetzungsverhältnis	-	4.5	6.25	8	11.5	15	20.25	28.12	36	50	64	91.12	126.5	162	225	288	400	512
Efficiency/ Wirkungsgrad	%	90				81						73						
Number of stages/ Stufenzahl		1				2						3						
Continuous torque/ Dauerdrehmoment	Nm	up to/ bis 1.2				up to/ bis 8						up to/ bis 24						
Weight of gearbox/ Getriebegewicht	kg	0.6				0.72						0.88						
Axial load/ radial load */ Axiallast/ Radiallast *	N	500 / 350				500 / 350						500 / 350						

Dimensions in mm/ Maßzeichnung in mm

Depending on the motor type, the mounting pattern may be rotated by 45°. Please ask us for details/
Je nach Motortyp kann die Anbaulage um 45° gedreht sein. Bitte fragen Sie uns nach Details.

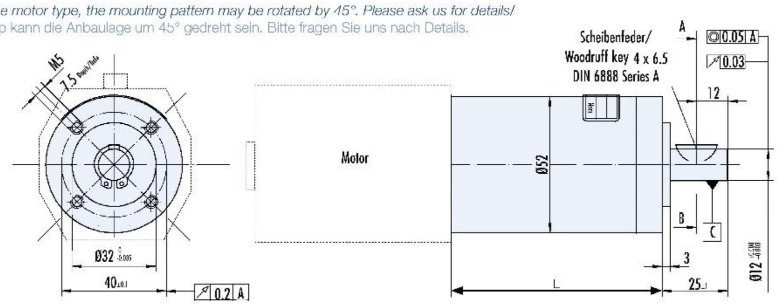

Length/ Länge L mm	
1-stufig/ stage	50
2-stufig/ stage	65.5
3-stufig/ stage	80.5

200 | *Visit www.dunkermotoren.com for further product information/* Besuchen Sie www.dunkermotoren.de für weitere Produktinformationen

Appendix I – Electromagnetic brake SWB-03

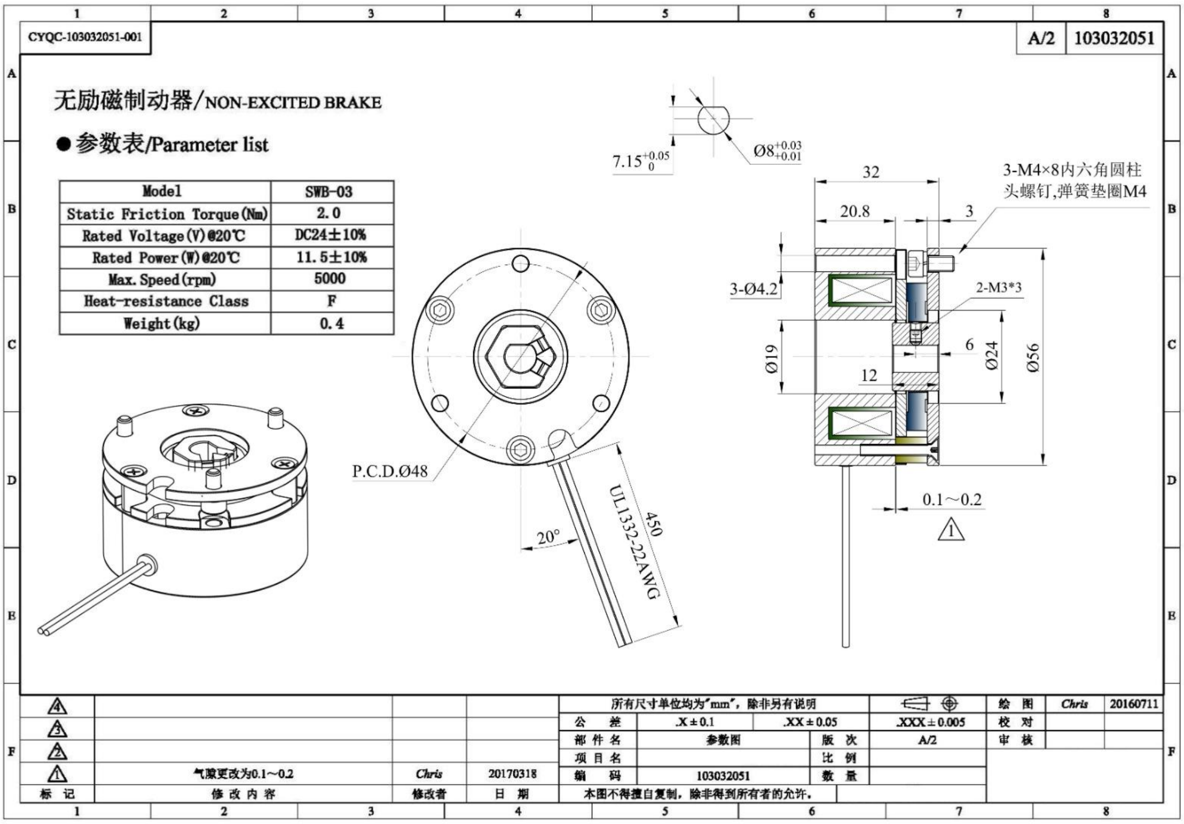

Appendix J– Dunkermotoren Stepper motor ST 17 | 634 017 | Nema 17 17X14

ST 17 | 634 017 | *Nema 17 stepper motor*

- 2 Phase Hybrid Stepper
- 1.8° step angle (+/-5%)
- 42 mm square Nema 17
- High grade Neodymium magnets
- Customized solutions available on demand
- Operating temperatures -20°C to +40°C
- Sinusoidal back EMF optimized for microstep operation and high holding torque
- Insulation Class 130 (B)

Data		17x14	17x14	17x14	17x16	17x16	17x16	17x20	17x20	17x20
Rated phase current	A	0,40	1,00	1,50	0,40	1,00	2,00	0,40	1,00	2,00
Phase resistance	Ohm	17,9	3,45	1,49	21,21	3,38	0,96	24,88	3,87	1,09
Phase inductance	mH	26,25	4,82	2,02	38,95	6,53	1,69	43,80	7,05	1,64
Holding torque bipolar	Ncm	27	29	28	46	46	46	57	57	57
Detent torque	Ncm	2	2	2	2	2	2	2,5	2,5	2,5
Rotor inertia	gcm²	40	40	40	57	57	57	83	83	83
Max voltage	VDC	50	50	50	50	50	50	50	50	50
Weight	Kg	0,24	0,24	0,24	0,30	0,30	0,30	0,41	0,41	0,41

all data measured with standard cables 300 mm at 25°C

Modular System

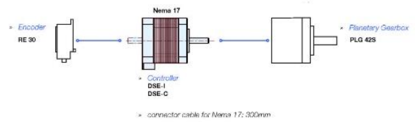

- connector cable for Nema 17: 300mm

48 | Visit www.ametekmae.com for further product information

ST 17 | 634 017 | *Nema 17 stepper motor*

Dimensions in mm

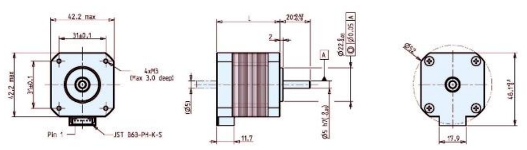

- Shaft D cut option: 4.5X15 mm
- Radial connector available upon request

Motor	L
17x14	36.3±0.6
17x16	41.1±0.6
17x20	53.0±0.6

Characteristic diagram

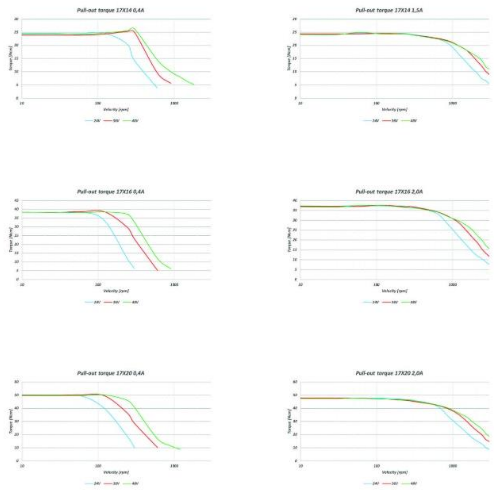

Visit www.ametekmae.com for further product information

Appendix K – Dunker motoren Gearbox with 2 stages PLG 42 S

» PLG 42 S

- *Compact, industry compatible planetary gearbox*
- *Output shaft with dual ball bearings*
- *All stages have straight toothing*

- Kompaktes, industrietaugliches Planetengetriebe
- Ausgangswelle doppelt kugelgelagert
- Alle Getriebestufen geradverzahnt ausgeführt

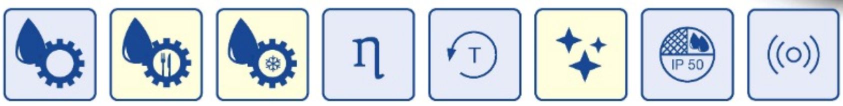

Lifetime lubrication | *Food grade lubrication* | *Low temperature* | *High efficiency* | *High torque* | *Special surface available* | *Protection class (up to)* | *Vibration resistance*

Data/ Technische Daten | PLG 42 S - *Ring gear made of steel/* Hohlrad aus Stahl

Reduction ratio/ Untersetzungsverhältnis	-	4	6.25	8	16	25	32	50	64	100	128	156.25	200	256	312.5	400	512
Efficiency/ Wirkungsgrad	%	90			81					73							
Number of stages/ Stufenzahl	-	1			2					3							
Continuous torque/ Dauerdrehmoment	Nm	*up to/* bis 0.7 (*no metallic planet gears/* Kunststoff-Planetenräder) / 3.5			*up to/* bis 6					*up to/* bis 14							
Weight of gearbox/ Getriebegewicht	kg	0.27			0.37					0.47							
*Axial load/ radial load */* Axiallast/ Radiallast *	N	150 / 250			150 / 250					150 / 250							

* *From center of shaft/* Ab Wellenmitte

Dimensions in mm/ Maßzeichnung in mm

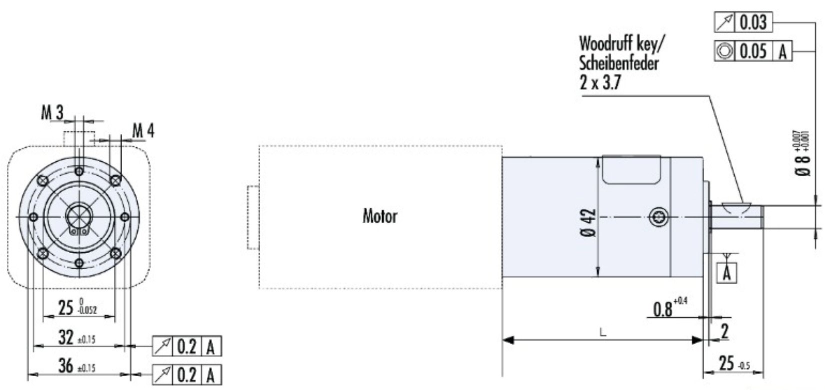

Depending on the motor type, the mounting pattern may be rotated by 45°. Please ask us for details/ Je nach Motortyp kann die Anbaulage um 45° gedreht sein. Bitte fragen Sie uns nach Details.

Length/ Länge L mm	
1-stufig/ stage	46.8
2-stufig/ stage	58.6
3-stufig/ stage	70.4

198 | *Visit www.dunkermotoren.com for further product information/* Besuchen Sie www.dunkermotoren.de für weitere Produktinformationen

Appendix L – ShenZhen ZhongLing Technology ZLLG65ASM250-L (Double shaft)



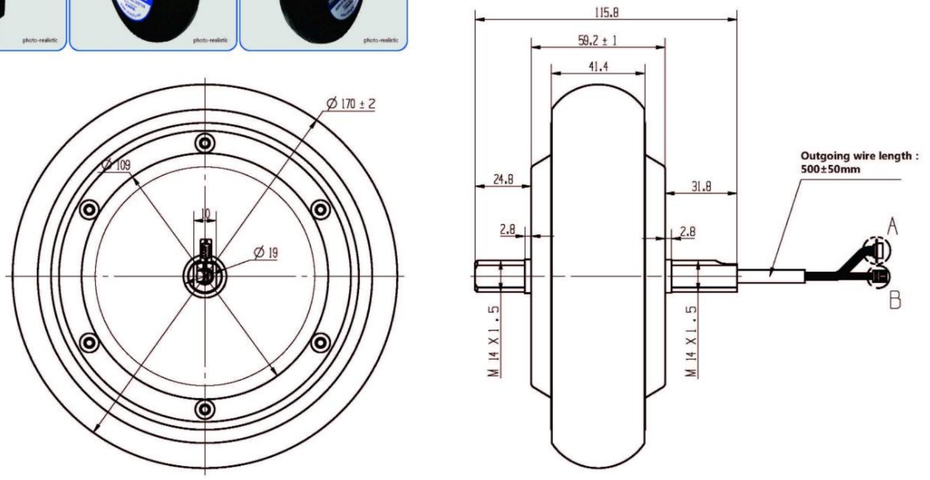

Rated Voltage	Power	Rated Torque	Maximum Torque	Rated Speed	Maximum Speed	Rated Phase Current	Max Phase Current
24VDC	150W	6.5N.m	13N.m	200RPM	260RPM	4A	8A
Wheel Diameter	**Weight**	**Shaft Type**	**Encoder**	**Tire**	**Brake Type**	**Protection Level**	**Suggested Load**
170mm	3KG	Double shaft	1024-wire optical encoder	Rubber	Electric brake	IP54	120KG

Power Wire			
Pin	1	2	3
Color	Blue	Yellow	Green
Signal	Power Wire W	Power Wire U	Power Wire V

Signal Wire							
Pin	5	4	3	2	1	8	7
Color	Blue	Green	Yellow	Red	Black	Purple	White
Signal	Hall V	Hall U	Hall W	+5V	GND	Encoder A+	Encoder B+

Temperature Sensor	
NC	NC
Brown	Grey
Thermistor +	Thermistor -

ZLTECH®	Design change	1		View		Design:	Date:	Company Name: **ShenZhen ZhongLing Technology Co., Ltd**
		2				Proofread:	Date:	Product Name: **Hub Servo Motor**
		3						
		4		ERP:		Approve:	Date:	Product P/N: **ZLLG65ASM250-L(Double shaft)**

Appendix M - EVVA EV1865PACK 40Ah

https://www.alibaba.com/product-detail/Long-Cycle-Life-24v-40ah-Lithium_1600092102834.html

PRODUCT ATTRIBUTE

Application	Toys, Power Tools, Home Appliances, Boats, Electric Bicycles/Scooters, Electric Folklifts, Electric Vehicles, Electric Wheelchairs, Electric scooter
Battery Size	LITHIUM ion battery
Brand Name	EVVA
Certification	ce msds
Model Number	EV1865PACK
Place of Origin	China
China	Guangdong
Weight	6.4kg
Type	Li-Ion
Composed Type	7S10P
Size	372*140*70mm
Nominal Voltage	25.2V
Cell origin	A Grade Li-ion cells from Japan, Korea and Singapore
Cycle life	over 1000 Times
BMS	Built-in protection circuit
Charge Voltage	29.4V
Max discharge current	10~30A
Discharge Cut-off Voltage	19V

Appendix N – SKF 7203 BE-2RZP

7203 BE-2RZP

Single row angular contact ball bearing with 40° contact angle and non-contact seals on both sides

These single row angular contact ball bearings, with 40° contact angle and non-contact seals on both sides, accommodate radial and axial loads acting simultaneously, where the axial load acts in one direction only. They have a ball-centred glass-fibre reinforced PA66 cage. They are more suitable than deep groove ball bearings for supporting large axial forces acting in one direction.

- 40° contact angle
- Integral sealing prolongs bearing service life
- Glass-fibre reinforced PA66 cage
- Accommodate relatively high radial loads and large unilateral axial loads

Overview

Dimensions

Bore diameter	17 mm
Contact angle	40 °
Outside diameter	40 mm
Width	12 mm

Performance

Basic dynamic load rating	10.4 kN
Basic static load rating	5.5 kN
Limiting speed	17 000 r/min
Reference speed	22 000 r/min

Properties

Axial internal clearance	Not applicable
Cage	Non-metallic
Coating	Without
Contact type	Normal contact (two-point contact)
Locating feature, bearing outer ring	None
Lubricant	Grease
Matched arrangement	No
Material, bearing	Bearing steel
Number of rows	1
Relubrication feature	Without
Ring type	One-piece inner and outer rings
Sealing	Seal on both sides

Technical Specification

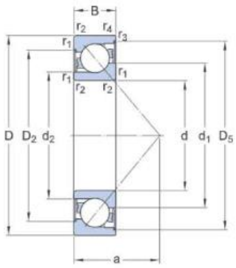

Dimensions

d	17 mm	Bore diameter
D	40 mm	Outside diameter
B	12 mm	Width
d_1	≈ 26.25 mm	Shoulder diameter of inner ring (large side face)
d_2	≈ 21.66 mm	Shoulder diameter of inner ring (small side face)
D_2	≈ 34 mm	Recess diameter of outer ring (large side face)
a	18 mm	Distance side face to pressure point
$r_{1,2}$	min. 0.6 mm	Chamfer dimension
$r_{3,4}$	min. 0.6 mm	Chamfer dimension

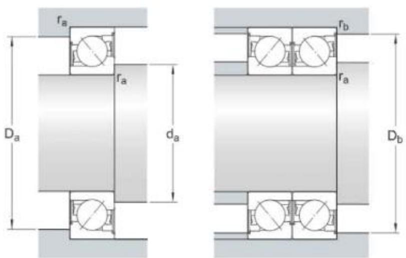

Abutment dimensions

d_a	min. 21.2 mm	Diameter of shaft abutment
d_a	max. 26.25 mm	Diameter of shaft abutment
D_a	max. 35.8 mm	Abutment diameter housing
D_b	max. 35.8 mm	Diameter of housing abutment
r_a	max. 0.6 mm	Radius of fillet
r_b	max. 0.6 mm	Radius of fillet

Calculation data

Basic dynamic load rating	C	10.4 kN
Basic static load rating	C_0	5.5 kN
Fatigue load limit	P_u	0.236 kN
Reference speed		22 000 r/min

Limiting speed		17 000 r/min
Minimum axial load factor	A	0.000625
Minimum radial load factor	k_r	0.095
Limiting value	e	1.14

Single bearing or bearing pair arranged in tandem

Radial load factor (single, tandem)	X	0.35
Axial load factor (single, tandem)	Y_0	0.26
Axial load factor (single, tandem)	Y_2	0.57

Bearing pair arranged back-to-back or face-to-face

Radial load factor (back-to-back, face-to-face)	X	0.57
Axial load factor (back-to-back, face-to-face)	Y_0	0.52
Axial load factor (back-to-back, face-to-face)	Y_1	0.55
Axial load factor (back-to-back, face-to-face)	Y_2	0.93

Mass

Mass	0.063 kg

Sealing type	Non-contact
Universal matching bearing	No